Autophagy

ISSN: (Print) (Online) Journal homepage: https://www.tandfonline.com/loi/kaup20

Protective effect of the tunneling nanotube-TNFAIP2/M-sec system on podocyte autophagy in diabetic nephropathy

F. Barutta, S. Bellini, S. Kimura, K. Hase, B. Corbetta, A. Corbelli, F. Fiordaliso, S. Bruno, L. Biancone, A. Barreca, M.G. Papotti, E. Hirsh, M. Martini, R. Gambino, M. Durazzo, H. Ohno & G. Gruden

To cite this article: F. Barutta, S. Bellini, S. Kimura, K. Hase, B. Corbetta, A. Corbelli, F. Fiordaliso, S. Bruno, L. Biancone, A. Barreca, M.G. Papotti, E. Hirsh, M. Martini, R. Gambino, M. Durazzo, H. Ohno & G. Gruden (2022): Protective effect of the tunneling nanotube-TNFAIP2/M-sec system on podocyte autophagy in diabetic nephropathy, Autophagy, DOI: 10.1080/15548627.2022.2080382

To link to this article: https://doi.org/10.1080/15548627.2022.2080382

AUTOPHAGY
https://doi.org/10.1080/15548627.2022.2080382

Taylor & Francis
Taylor & Francis Group

RESEARCH PAPER

Protective effect of the tunneling nanotube-TNFAIP2/M-sec system on podocyte autophagy in diabetic nephropathy

F. Barutta [a,*], S. Bellini [a,*], S. Kimura[b], K. Hase[b], B. Corbetta[a], A. Corbelli[c], F. Fiordaliso[c], S. Bruno[a], L. Biancone[a], A. Barreca[d], M.G. Papotti[e], E. Hirsh [f], M. Martini [f], R. Gambino[a], M. Durazzo[a], H. Ohno[g], and G. Gruden [a]

[a]Department of Medical Sciences, University of Turin, Turin, Italy; [b]Division of Biochemistry, Faculty of Pharmacy, Keio University, Tokyo, Japan; [c]Unit of Bioimaging, Department of Molecular Biochemistry and Pharmacology, Istituto di Ricerche Farmacologiche Mario Negri IRCCS, Milan, Italy; [d]Division of Pathology, Città della Salute e della Scienza Hospital, Turin, Italy; [e]Department of Oncology, University of Turin, Turin, Italy; [f]Department of Molecular Biotechnology and Health Sciences, University of Turin, Turin, Italy; [g]Laboratory for Intestinal Ecosystem, RIKEN Center for Integrative Medical Sciences, Yokohama, Japan

ABSTRACT

Podocyte injury leading to albuminuria is a characteristic feature of diabetic nephropathy (DN). Hyperglycemia and advanced glycation end products (AGEs) are major determinants of DN. However, the underlying mechanisms of podocyte injury remain poorly understood. The cytosolic protein TNFAIP2/M-Sec is required for tunneling nanotubes (TNTs) formation, which are membrane channels that transiently connect cells, allowing organelle transfer. Podocytes express TNFAIP2 and form TNTs, but the potential relevance of the TNFAIP2-TNT system in DN is unknown. We studied TNFAIP2 expression in both human and experimental DN and the renal effect of *tnfaip2* deletion in streptozotocin-induced DN. Moreover, we explored the role of the TNFAIP2-TNT system in podocytes exposed to diabetes-related insults. TNFAIP2 was overexpressed by podocytes in both human and experimental DN and exposure of podocytes to high glucose and AGEs induced the TNFAIP2-TNT system. In diabetic mice, *tnfaip2* deletion exacerbated albuminuria, renal function loss, podocyte injury, and mesangial expansion. Moreover, blockade of the autophagic flux due to lysosomal dysfunction was observed in diabetes-injured podocytes both *in vitro* and *in vivo* and exacerbated by *tnfaip2* deletion. TNTs allowed autophagosome and lysosome exchange between podocytes, thereby ameliorating AGE-induced lysosomal dysfunction and apoptosis. This protective effect was abolished by *tnfaip2* deletion, TNT inhibition, and donor cell lysosome damage. By contrast, *Tnfaip2* overexpression enhanced TNT-mediated transfer and prevented AGE-induced autophagy and lysosome dysfunction and apoptosis. In conclusion, TNFAIP2 plays an important protective role in podocytes in the context of DN by allowing TNT-mediated autophagosome and lysosome exchange and may represent a novel druggable target.

Abbreviations: AGEs: advanced glycation end products; AKT1: AKT serine/threonine kinase 1; AO: acridine orange; ALs: autolysosomes; APs: autophagosomes; BM: bone marrow; BSA: bovine serum albumin; CTSD: cathepsin D; DIC: differential interference contrast; DN: diabetic nephropathy; FSGS: focal segmental glomerulosclerosis; HG: high glucose; KO: knockout; LAMP1: lysosomal-associated membrane protein 1; LMP: lysosomal membrane permeabilization; MAP1LC3/LC3: microtubule-associated protein 1 light chain 3; PI3K: phosphoinositide 3-kinase; STZ: streptozotocin; TNF: tumor necrosis factor; TNFAIP2: tumor necrosis factor, alpha-induced protein 2; TNTs: tunneling nanotubes; WT: wild type.

ARTICLE HISTORY
Received 17 February 2022
Revised 11 May 2022
Accepted 17 May 2022

KEYWORDS
Advanced glycation end products; albuminuria; autophagosomes; experimental diabetes; hyperglycemia; lysosomes; nephrin; podocytes; renal function loss; slit diaphragm

Introduction

Diabetic nephropathy (DN), a chronic complication of diabetes, is the leading cause of end-stage renal disease (ESRD) in the western world. The complication is characterized by both albuminuria and progressive renal function loss [1,2]. These functional alterations are primarily due to both excessive accumulation of extracellular matrix in the mesangium and podocyte damage.

Podocytes form the glomerular filtration barrier together with the glomerular basement membrane and the fenestrated glomerular endothelium. The junction between adjacent podocyte foot processes (FP), named slit diaphragm (SD), is the major restriction site to protein filtration in the glomeruli. Downregulation of SD proteins, such as NPHS1/Nephrin and NPHS2/Podocin, FP effacement, and podocyte apoptosis are early features of DN and major determinants in the development of albuminuria [3–6].

Both hyperglycemia and advanced glycation end products (AGEs) play an important role in the pathogenesis of the podocyte injury in DN by inducing both oxidative stress and inflammation [7–9]. In addition, dysfunction of intracellular organelles also contributes to podocyte damage [10–15]. However, the mechanisms underlying podocyte impairment in DN are not fully understood. Moreover, most studies

CONTACT F. Barutta federica.barutta@unito.it Department of Medical Sciences, Corso Dogliotti 14 10126, Turin, Italy
*co-first authors

Supplemental data for this article can be accessed online at https://doi.org/10.1080/15548627.2022.2080382

focussed on mechanisms of podocyte damage and relatively little is known on counteracting mechanisms of cytoprotection.

Tunneling nanotubes (TNTs) are open-ended straight membrane channels (20–500 nm) without contact to the substrate that interconnect cells over long distances [16–20]. These intercellular bridges have been demonstrated in a variety of cell types *in vitro* [21–26] and more recently *in vivo* [27–31]. Cells form TNTs *de novo* in response to various stresses, including serum deprivation, hypoxia, oxidative stress, and inflammation [24,32–38]. TNTs allow horizontal intercellular transfer of cellular components, including small organelles, such as mitochondria, endosomes, and lysosomes, to target cells [39–44]. Replacement of damaged organelles via TNTs increases resistance of recipient cells to injury.

The protein TNFAIP2/M-Sec (tumor necrosis factor, alpha-induced protein 2) plays a crucial role in TNT formation by interacting with the exocyst complex and triggering polymerization of F-actin [45–47]. Expression of TNFAIP2 is observed predominantly in immune, endothelial, and cancer cells, and it is enhanced by both retinoic acid and inflammatory cytokines, including TNF/TNF-α [48–53]. There is little information on the TNFAIP2-TNT system in the kidney. However, podocytes can express TNFAIP2 and their exposure to either serum deprivation or adriamycin induces a TNFAIP2-TNT-dependent transfer of mitochondria from healthy to injured podocytes [54]. In addition, *in vivo* deletion of *Tnfaip2* causes the spontaneous development of focal segmental glomerulosclerosis (FSGS) in the susceptible BALB/c mouse strain [54].

Whether diabetes-induced cellular stress activates the TNFAIP2-TNT system in podocytes and if this system confers protection to podocytes by organelle exchange has not yet been explored.

Therefore, in the present study, we assessed podocyte TNFAIP2 expression in both human and experimental DN, investigated the effect of *tnfaip2* deletion in experimental DN, and explored *in vitro* in diabetes-injured podocytes the mechanism of TNFAIP2-TNT-mediated cytoprotection.

Results

TNFAIP2 expression in human and experimental DN

TNFAIP2 expression was studied in renal biopsies obtained from patients with DN and non-diabetic control subjects (Table 1). Glomerular immunostaining for TNFAIP2 was fourfold greater in patients with DN compared to controls (Figure 1(A)). The pattern of staining suggested a predominant podocyte distribution, as confirmed by colocalization of TNFAIP2 and the podocyte marker SYNPO (synaptopodin) in double immunofluorescence (Figure 1(B)). Of interest, an increased TNFAIP2 expression was also observed in kidney biopsies from patients with microalbuminuria.

Consistent with this, a significant increase in both immunostaining for TNFAIP2 and *Tnfaip2* mRNA levels was observed in the glomeruli from C57BL/6 mice after 12 weeks of streptozotocin (STZ)-induced diabetes (Figure 1(C-E)). Moreover, podocytes were the main cell type overexpressing TNFAIP2 within the diabetic glomeruli, as shown by immunostaining for TNFAIP2 and NPHS2 in serial cortex sections (Figure 1(F)). Of interest, a significant increase in *Tnfaip2* mRNA levels was also observed in isolated glomeruli in a very early stage (6 weeks) of experimental diabetes (control animals: 0.57 ± 0.07; diabetic mice: 1.19 ± 0.09; $p < 0.01$).

Table 1. Clinical parameters of patients with diabetic kidney disease (DKD) and non-diabetic control subjects.

	Controls	DKD
N	8	15
Age (years)	65.4 ± 6.3	66.5 ± 2.8
Sex (male/female)	6/2	11/4
Diabetes duration (years)	-	19.5 ± 0.7
Systolic blood pressure (mmHg)	120 ± 2.2	143 ± 4.6
Diastolic blood pressure (mmHg)	65 ± 3.1	83 ± 4.2
Serum creatinine (mg/dl)	1 ± 0.1	2.1 ± 0.4
Proteinuria (g/24 h)	-	2.1 ± 0.5
Hypertension (%)	-	100

Data are expressed as mean ± SEM

Effect of diabetes-related insults on the TNFAIP2-TNT system in cultured podocytes

To explore the underlying mechanism of TNFAIP2 overexpression, cultured podocytes were exposed to diabetes-related insults. Podocyte incubation in a high glucose (HG) (25 mM) milieu induced an over twofold increase in TNFAIP2 expression via a PI3K (phosphoinositide 3-kinase)-dependent mechanism (Figure 1(G, H)), while no changes were observed in response to AGE-bovine serum albumin (BSA) and mechanical stretch, mimicking glomerular capillary hypertension (Figure 1(I, J)). HG-induced PI3K-dependent *Tnfaip2* expression occurred via a transcriptional mechanism as PI3K inhibition using LY294002 (LY) also prevented *Tnfaip2* mRNA expression (NG: 1.0 ± 0.01; NG + LY: 1.14 ± 0.09; HG: 2.81 ± 0.52; HG + LY: 1.24 ± 0.26).

Given the key role of TNFAIP2 in TNT formation, we next investigated if diabetes-related insults can also promote TNT formation. Exposure to either HG or AGE-BSA caused formation of TNT-like structures that fulfilled the morphological criteria of TNTs, including the lack of contact to the substrate and the presence of an actin backbone (Figure 2(A-D)). Importantly, both HG and AGE-BSA increased the number of podocytes connected by TNTs in a PI3K-AKT1-dependent and TP53/TRP53/P53-independent manner (Figure 2(E, F)). *Tnfaip2* silencing completely prevented diabetes-induced TNT formation (Figure 2(G-I)), confirming that TNFAIP2 is required for TNT development.

Diabetes induction in tnfaip2-knockout (KO) C57BL/6 mice

To assess the functional relevance of TNFAIP2 *in vivo*, we knocked out *Tnfaip2* in C57BL/6 mice, a strain that is susceptible to STZ-induced diabetes, but resistant to FSGS. Homozygous *tnfaip2* KO C57BL/6 mice were viable, born at normal Mendelian ratios, and grew normally. There were no differences in albuminuria, renal function, and glomerular structure between *tnfaip2* KO and wild type (WT) animals even after long term follow-up (26 weeks of age). Therefore,

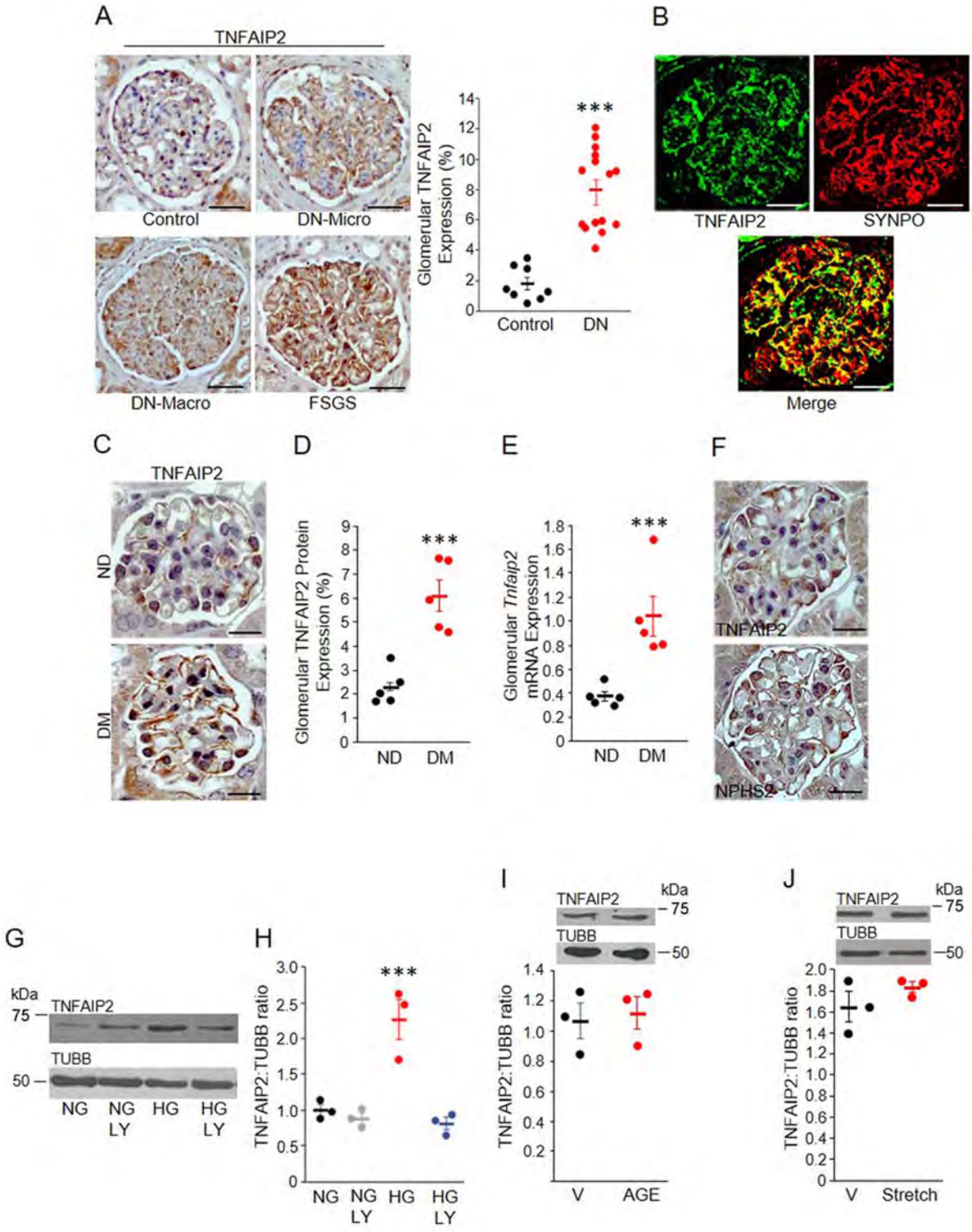

Figure 1. TNFAIP2 expression in both human and experimental diabetic nephropathy. (A) Glomerular TNFAIP2 protein expression was assessed by immunohistochemistry in renal cortex sections from control subjects (n = 8) and patients with either incipient (DN-micro, n = 3) or overt diabetic nephropathy (DN-macro, n = 12) (original magnification 200X, scale bar: 100 µm). Focal segmental glomerulosclerosis (FSGS) sections were used as a positive control. The percent area of positive staining is shown in the graph (***p < 0.001 DN vs. control). (B) Double immunofluorescence for TNFAIP2 and the podocyte marker SYNPO (synaptopodin) was carried out on renal sections from DN patients. The merged image shows colocalization (original magnification 200X, scale bar: 100 µm). (C) Representative immunohistochemistry images of glomerular TNFAIP2 protein expression in renal cortex sections from non-diabetic (ND) and diabetic mice (DM) after 12 weeks of diabetes (magnification 400X, scale bar: 50 µm). (D) The graph shows the percent area of glomerular TNFAIP2-positive staining (n = 5 mice per group; ***p < 0.001 DM vs. ND). (E) *Tnfaip2* mRNA levels were measured in the glomeruli isolated from ND and DM mice by real time-PCR and results corrected for the expression of the housekeeping gene *Hprt* (n = 5 mice per group; ***p < 0.001 ND vs. DM). (F) Staining for NPHS2/Podocin and TNFAIP2 on serial renal cortical sections obtained from DM mice showed a podocyte distribution (magnification 400X, scale bar: 50 µm). (G) Representative immunoblotting of TNFAIP2 in cultured podocytes exposed to high glucose concentrations (HG) for 48 h with and without the PI3K inhibitor, LY294002 (LY). TUBB/Tubulin was used as a loading control. (H) Results of densitometry analysis are shown in the graph (n = 3; ***p < 0.001 HG vs. others). (I and J) Immunoblottings showing TNFAIP2 expression in podocytes exposed to AGEs, mechanical stretch (10% elongation) or vehicle (V). Results of densitometry analyses are shown in the graphs (p = ns).

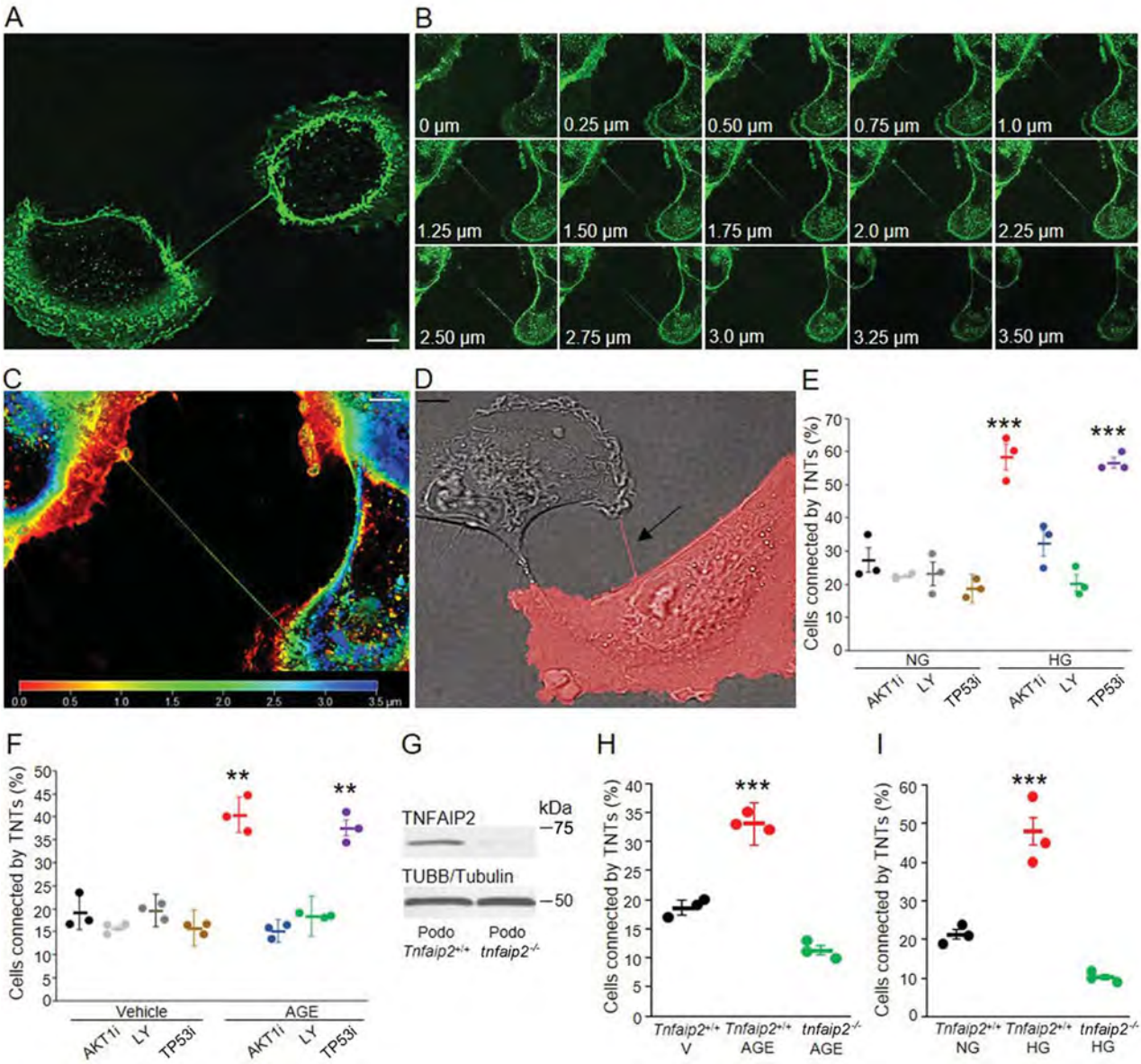

Figure 2. The TNFAIP2-TNT system in cultured podocytes exposed to diabetes-related insults. (A) Podocytes pre-exposed to high glucose concentrations (HG) for 48 h were stained with wheat germ agglutinins (WGA) Alexa Fluor 488 to reveal TNTs. A representative image showing a TNT-like channel, interconnecting two podocytes, is shown (magnification 630X, scale bar: 50 µm). (B) Serial Z-stack images, acquired with a step-size of 0.25-µm proved that TNTs did not adhere to the substrate. In panel C, colors represent the Z-depth (depth coding; red: bottom, blue: top). (D) F-actin was labeled with Cell-Light Actin-RFP to show that TNTs have an actin backbone (magnification 630X, scale bar: 50 µm). (E and F) Podocytes were exposed to normal (NG) or high glucose (HG) (E) and vehicle or AGEs (F) with and without inhibitors of AKT1 (AKT1-VIII inhibitor (AKT1i); 1 µM), PI3K (LY-294002 (LY); 50 µM), and TP53 (p-nitro-pifithrin (TP53i); 5 µM), stained with WGA Alexa Fluor 488, and analyzed by fluorescent live cell microscopy. The graphs show the percentage of podocytes connected by one or more TNTs ($n = 3$; ***$p < 0.001$ HG and HG+p53i vs. others; **$p < 0.01$ AGEs and AGEs+p53i vs. others). (G) Murine podocytes were transfected with either *Tnfaip2* shRNA (*tnfaip2*$^{-/-}$) or a mock plasmid (*Tnfaip2*$^{+/+}$). Knockdown efficiency was assessed by immunoblotting and TUBB/tubulin used as internal control. (h and i) *tnfaip2*$^{-/-}$ and *Tnfaip2*$^{+/+}$ podocytes were exposed to (H) vehicle or AGEs and (I) NG or HG for 48 h, stained with WGA Alexa Fluor 488, and analyzed by fluorescent live cell microscopy to reveal TNTs. The graphs show the percentage of podocytes connected by one or more TNTs (***$p < 0.001$ *Tnfaip2*$^{+/+}$ HG and *Tnfaip2*$^{+/+}$AGEs vs. others).

tnfaip2 deletion *per se* did not induce a renal phenotype in this strain (Fig. S1).

We then induced diabetes by STZ administration in both WT and *tnfaip2* KO C57BL/6 mice. Twelve weeks after diabetes onset, diabetic WT and *tnfaip2* KO mice had comparable values of blood glucose, glycated hemoglobin, body weight, kidney weight-to-body weight ratio, and systolic blood pressure. *tnfaip2* deletion did not affect albuminuria in non-diabetic mice, but significantly enhanced the rise in ALB (albumin):creatinine ratio (ACR) induced by diabetes. Furthermore, a significant reduction in creatinine clearance was exclusively observed in diabetic *tnfaip2* KO mice (Table 2), indicating that *Tnfaip2* abrogation worsened functional parameters of DN.

Structural abnormalities in diabetic tnfaip2 KO C57BL/6 mice

Histological assessment by periodic acid Schiff (PAS) staining revealed a mild mesangial expansion in diabetic mice. The degree of glomerular injury was greater in diabetic *tnfaip2* KO

Table 2. Metabolic and physiological parameters in WT and *tnfaip2* KO mice.

	ND-WT	ND-*tnfaip2* KO	DM-WT	DM-*tnfaip2* KO
Body weight (g)	30.20 ± 0.97	28.92 ± 1.73	21.65 ± 1.31[a]	20.80 ± 0.86 [a]
Blood glucose (mg/dl)	136.20 ± 2.80	150.70 ± 8.30	403.30 ± 40.1 [a]	382.50 ± 23.90 [a]
Glycated Hb (%)	4.75 ± 0.15	5.12 ± 0.10	10.92 ± 0.55 [a]	11.41 ± 0.33 [a]
SBP (mmHg)	108.00 ± 3.20	105.00 ± 3.10	103.00 ± 1.30	106.00 ± 2.50
KW:BW ratio	6.61 ± 0.32	5.45 ± 0.21	7.57 ± 2.11[b]	7.45 ± 0.42[b]
ACR (µg/mg)	36.80 ± 7.70	28.80 ± 7.90	68.20 ± 14.00[a]	144.10 ± 36.50[c]
CrCl (ml/min)	0.43 ± 1.37	0.40 ± 3.20	0.31 ± 3.74	0.17 ± 0.050[d]

Data are expressed as mean ± SEM; ND: non-diabetic; DM: diabetic; KW:BW: kidney weight:body weight; SBP: systolic blood pressure; ACR: ALB (albumin)-to-creatinine ratio; CrCl: creatinine clearance; [a]p<0.001; [b]p<0.05 DM groups vs. ND groups; [c]p<0.05 DM-*tnfaip2* KO vs. DM-WT; [d]p<0.05 DM-*tnfaip2* KO vs. others.

mice with a more prominent mesangial expansion, as assessed by both light and electron microscopy (Figure 3(A-C)). Furthermore, diabetes-induced overexpression of both FN1 (fibronectin 1) and the prosclerotic cytokine *Tgfb1* (transforming growth factor, beta 1) was enhanced in mice lacking *Tnfaip2* (Figure 3(D-F)).

Glomerular inflammation in diabetic tnfaip2 KO mice and chimeric animals

Diabetes induced glomerular infiltration of LGALS3/MAC2$^+$ (lectin, galactose binding, soluble 3) macrophages and an increased expression of *Ly6c2* (lymphocyte antigen 6 complex, locus C2) a marker of inflammatory monocytes. Moreover, overexpression of *Ccl2/MCP-1* (chemokine (C-C motif) ligand 2) and its cognate receptor *Ccr2* (chemokine (C-C motif) receptor 2) was also observed, indicating activation of the CCL2-CCR2 system that play a key role in monocyte accrual in the diabetic glomeruli. These proinflammatory effects were magnified in diabetic *tnfaip2* KO mice (Figure 3(G-J)). Surprisingly, expression of *Tnf*, which is known to induce TNFAIP2, was not affected by either diabetes or *tnfaip2* deletion (Figure 3(K)).

Although TNFAIP2 is expressed by inflammatory cells, our study in chimeric animals showed that transplantation of bone marrow (BM) cells of WT mice in diabetic *tnfaip2* KO mice did not ameliorate albuminuria and mesangial expansion (Table 3 and Figure 3(L-O)). This indicates that lack of *Tnfaip2* in BM cells did not play a primary role in explaining worsening of DN in *tnfaip2* KO mice. Genotyping confirmed reconstitution of *Tnfaip2* in peripheral blood cells of chimeric *tnfaip2* KO mice transplanted with BM from WT animals (Figure 3(M)).

Effect of diabetes and/or tnfaip2 deletion on podocytes

There were no podocyte abnormalities in non-diabetic *tnfaip2* KO mice. However, downregulation of both NPHS1/Nephrin and NPHS2/Podocin as well as FP effacement were observed in diabetic mice and exacerbated by *Tnfaip2* abrogation (Figure 4(A-D)). Moreover, both apoptosis and podocyte loss, as assessed by counting the number of CDKN1C$^+$ (cyclin-dependent kinase inhibitor 1C (P57)) cells, were only observed in diabetic *tnfaip2* KO mice (Figure 4(E, F)).

Consistent with these *in vivo* findings, exposure of cultured podocytes to AGE-BSA induced apoptosis and this was aggravated by both *Tnfaip2* deficiency and pre-incubation with latrunculin-B that prevents actin polymerization and thus TNT formation (Figure 4(G, H)). Therefore, lack of the TNFAIP2-TNT system appeared to sensitize podocytes to the deleterious effects of diabetes both *in vitro* and *in vivo*.

Effect of diabetes and/or tnfaip2 deletion on macroautophagy/autophagy

Autophagy is a key cellular mechanism for the degradation of dysfunctional organelles by sequestration within double-membrane vesicles autophagosomes (APs) and subsequent lysosomal fusion and degradation. We found that diabetes induced glomerular overexpression of the AP marker MAP1LC3/LC3 (microtubule-associated protein 1 light chain 3) (Figure 5(A)). Moreover, glomerular immunostaining for the autophagy receptor SQSTM1/p62 (sequestosome 1) was increased in diabetic mice, particularly in podocytes (Figure 5(D, C)). Similarly, exposure of cultured podocytes to either AGE-BSA or HG enhanced both LC3-II expression and the number of SQSTM1/p62$^+$-LC3$^+$ pucta (Figure 5(D-I)). These diabetes-induced alterations were magnified by *tnfaip2* deletion in both cultured podocytes and diabetic mice.

The concurrent rise in both LC3-II and SQSTM1/p62 together with the unchanged expression of the autophagy inducers *Becn1* (beclin 1, autophagy related), *Atg5* (autophagy related 5), and *Atg7* (autophagy related 7) (Figure 5(J-N)), suggested that *tnfaip2* deletion altered autophagy by inhibiting AP digestion.

Consistent with this, monitoring of the autophagic flux by tandem fluorescent-tagged LC3 (RFP-GFP-LC3) in AGE-BSA -treated podocytes showed that lack of *Tnfaip2* increased the number of APs (GFP$^+$ mRFP$^+$ yellow puncta), but reduced the number of red puncta (GFP$^-$mRFP$^+$) that form when yellow APs fuse with lysosomes and the green fluorescence of GFP is quenched by the low pH (Figure 6(A, B)). Importantly, a similar effect was also observed in AGE-BSA-treated WT podocytes pre-exposed to latrunculin-B indicating that both lack of *Tnfaip2* and inhibition of TNT formation can magnify abnormalities in AP clearance in the context of diabetes. The calculated GFP: RFP ratio was increased by exposure to AGEs and even further by *tnfaip2* deletion and latrunctulin B, indicating reduced autophagic flux (Figure 6(C)).

Effect of diabetes and/or tnfaip2 deletion on lysosomes

To establish if AP accumulation was due to either failure to fuse with lysosomes or inhibition of lysosomal acidification, we assessed fusion by double immunostaining for LC3 and the lysosome marker LAMP1 (lysosomal-associated

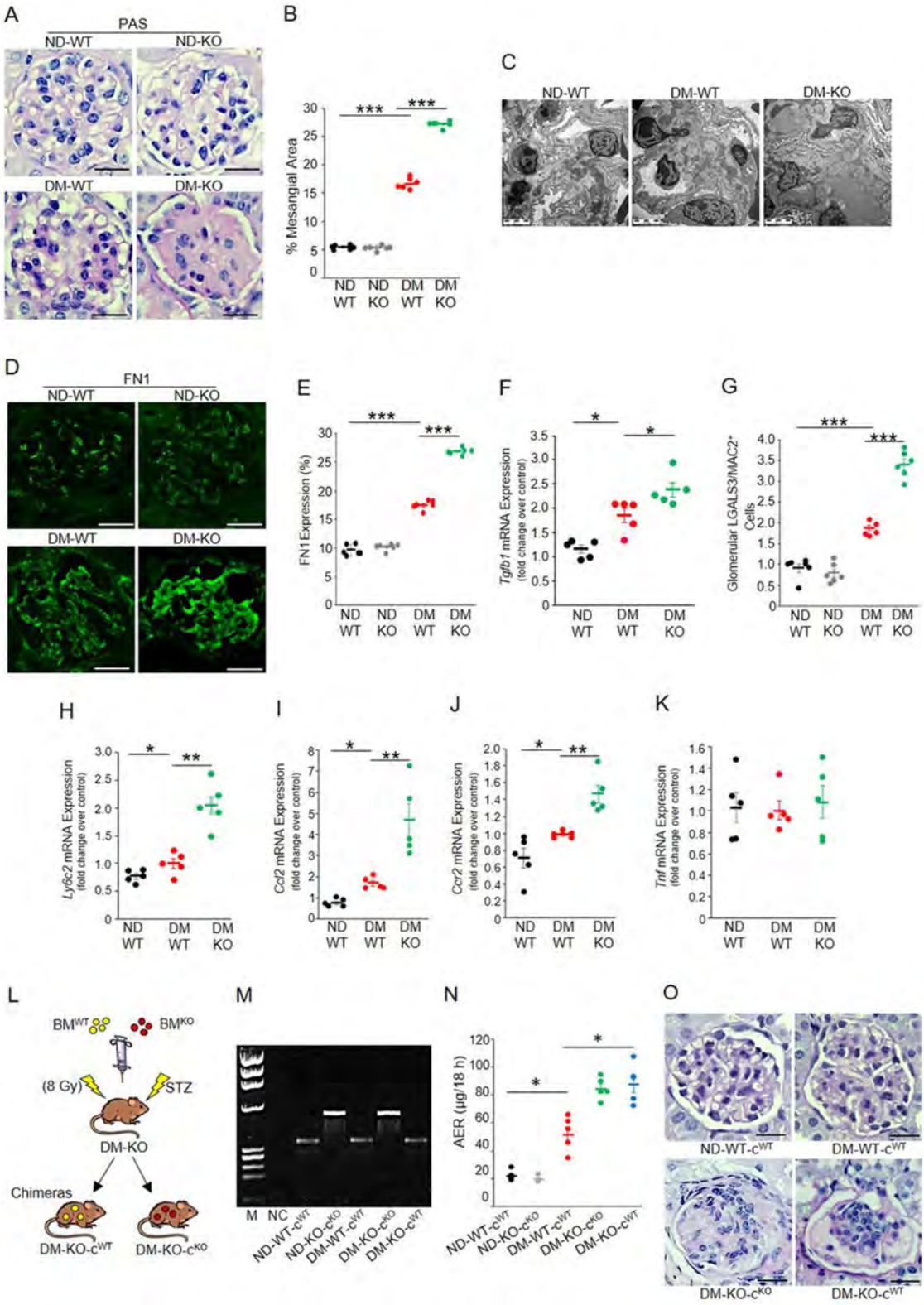

Figure 3. Effect of *tnfaip2* deletion on diabetes-induced glomerular structural abnormalities, markers of fibrosis, and inflammation. Renal cortex samples from diabetic (DM) and non-diabetic (ND) both WT (ND-WT, DM-WT) and *tnfaip2* KO (ND-KO, DM-KO) mice were studied 12 weeks after diabetes onset. (A) Representative periodic acid Schiff (PAS) staining images (magnification 400X, scale bar: 50 µm) and (B) quantification of glomerulosclerosis are shown (n = 6 mice per group; ***p < 0.001 DM-WT vs. ND-WT; DM-KO vs. DM-WT). (C) Electron microscopy images showing a more prominent mesangial expansion in the glomeruli from DM-KO mice compared to DM-WT mice (magnification 3200X). (D) Immunofluorescence images of glomerular FN1 (fibronectin 1) are shown (magnification 400X, scale bar: 50 µm). (E) Quantification of the percent area of glomerular FN1-positive staining (n = 6 mice per group; ***p < 0.001 DM-WT vs. ND-WT; DM-KO vs. DM-WT). (F) *Tgfb1* mRNA levels were measured by real-time PCR in total renal cortex and corrected for the expression of the housekeeping gene *Hprt* (n = 5 mice per group; *p < 0.05 DM-WT vs. ND-WT; DM-KO vs. DM-WT). (G) Glomerular macrophage accrual was evaluated by counting the number of LGALS3/MAC2-positive cells per glomerulus (n = 6 mice per group; ***p < 0.001 DM-WT vs. ND-WT; DM-KO vs. DM-WT). mRNA levels of *Ly6c2* (H), *Ccl2* (I), *Ccr2* (J), and *Tnf* (K) were measured in the renal cortex by real time-PCR and the results corrected for the expression of the housekeeping gene *Hprt* (n = 5 mice per group; *p < 0.05 DM-WT vs. ND-WT; **p < 0.01 DM-KO vs. DM-WT). (L) Schematic illustration of the protocol used for generating diabetic (DM) *tnfaip2* KO chimeric mice. Recipient *tnfaip2* KO mice were

membrane protein 1). There was a significant increase in the number of $LC3^{+}$ $LAMP1^{+}$ autolysosomes (ALs) in AGE-BSA treated podocytes compared to control cells and this diabetes-induced effect was magnified by *tnfaip2* deletion (Figure 6(D, E)). Therefore, AP-lysosome fusion was preserved and altered lysosome acidification was likely the predominant mechanism of AP accumulation.

Consistent with this, AGE-BSA-treated WT podocytes and to a greater extent AGE-treated *tnfaip2* KO cells showed a reduction in acridine orange (AO)-stained acidic organelles and an enhanced release of the lysosomal enzyme CTSD (cathepsin D) into the cytosol, which are both markers of lysosomal dysfunction and lysosomal membrane permeabilization (LMP) (Figure 7(A, B)). Moreover, activity of CTSD was significantly reduced in AGE-BSA-treated podocytes and even more in AGE-BSA-treated *tnfaip2* KO cells (Figure 7(E)). Re-expression of *Tnfaip2* abolished the deleterious effect of *tnfaip2* deletion on AGE-BSA-induced SQSTM1/p62 accumulation, LMP, CTSD activity (Figure 7(A-E)), and podocyte apoptosis (Figure 7(F, G)), confirming specificity of these findings.

TNT-TNFAIP2-mediated lysosome and AP transfer

To functionally link lysosome alterations to the TNFAIP2-TNT system, we next assessed whether TNTs can mediate transfer of lysosomes and APs between podocytes. Cell-Tracker Blue-labeled podocytes (recipients) were treated with AGE-BSA (100 µg/ml) and then co-cultured with normal podocytes (donors), containing green fluorescent protein (GFP)-labeled lysosomes. Fluorescent lysosomes were found along TNTs and in the cytosol of recipient blue cells, indicating lysosome transfer (Figure 8(A)) from healthy to AGE-BSA-treated cells. Flow cytometry analyses showed that TNT-mediated lysosome transfer towards AGE-BSA-treated podocytes was significantly increased. However, transfer was almost abolished when recipient podocytes were cocultured with donor podocytes either lacking *Tnfaip2* or pre-exposed to latrunculin-B, indicating a TNFAIP2-TNT-dependent phenomenon. Consistently, re-expression of *Tnfaip2* rescued the ability of KO podocytes to form TNTs (WT^{Adv-}: 19.54 ± 0.39; KO^{Adv-}: 8.32 ± 0.56; KO^{Adv+}: 17.43 ± 0.89, % of podocytes connected by TNTs; $p < 0.001$ KO^{Adv-} vs. others) and to exchange lysosomes and *Tnfaip2* overexpression even magnified lysosome transfer (Figure 8(B, C)). Of relevance, we also demonstrated transfer of lysosomes between podocytes exposed to different concentrations of AGEs (50 vs. 200 µg/ml) (Figure 8(D, E)). AP transfer in the opposite direction was observed from AGE-BSA-treated to normal podocytes (Figure 8(F)). As shown in Fig. S2, transfer was not limited to autophagy-related organelles and shuttling of mitochondria from normal podocytes to AGE-BSA-treated cells was also found.

Cytoprotective effect of the TNFAIP2-TNT system on AGE-treated podocytes

We then investigated the potential cytoprotective effect of TNFAIP2-TNT-mediated organelle exchange in WT diabetes-injured podocytes. In the co-culture system described above, we found that coincubation of AGE-BSA-injured podocytes with healthy donor podocytes not only enhanced lysosome transfer in a TNFAIP2-TNT dependent manner, but also reduced SQSTM1/p62 accumulation, LMP, and podocyte apoptosis in recipient cells. These protective effects of donor podocytes were magnified by *Tnfaip2* overexpression. On the contrary, benefit was no longer observed when leupeptin-treated podocytes, carrying altered lysosomes, were used as donor cells, confirming the importance of lysosome transfer in rescuing damaged cells (Figure 9).

Finally, overexpression of *Tnfaip2* in monoculture of AGE-exposed podocytes also improved SQSTM1/p62 accumulation, LMP, CTSD activity and significantly reduced podocyte apoptosis (Figure 10), indicating that benefit was observed even in the absence of exogenous healthy cells functioning as supplier of healthy organelles.

Discussion

Our study provides evidence that TNFAIP2 is overexpressed by podocytes in both human and experimental DN. Moreover, *tnfaip2* deletion exacerbated albuminuria, renal function loss, and structural abnormalities of experimental DN with evidence of enhanced both podocyte injury and impaired autophagy.

In humans, TNFAIP2 overexpression by podocytes was observed not only in patients with established DN, but also in individuals with microalbuminuria, though the number of subjects was small. This suggests that TNFAIP2 induction may be an early event in the natural history of DN. According with this, there was glomerular *Tnfaip2* overexpression in an early phase of experimental diabetes.

Podocyte overexpression of TNFAIP2 also occurs in FSGS [54], raising the hypothesis that TNFAIP2 induction may be a common response to podocyte injury. TNFAIP2 upregulation is likely a compensatory mechanism aimed to limit glomerular injury. Indeed, in our study *tnfaip2* deletion worsened podocyte injury. Moreover, BALB/c mice lacking *Tnfaip2* spontaneously develop podocyte damage, leading to FSGS with aging [54].

At variance with BALB/c mice, C57BL/6 *tnfaip2* KO mice did not have a renal phenotype in the absence of diabetes. The greater susceptibility to develop FSGS of BALB/c compared to C57BL/6 mice may provide explanation for this strain-dependent effect [55–57]. Lack of *Tnfaip2*, however, worsened experimental DN in C57BL/6 mice, implying that diabetes-induced glomerular

lethally irradiated, and then reconstituted with bone marrow (BM) from either WT (DM-KO-c^{WT}) or KO (DM-KO-c^{KO}) mice. (M) PCR genotyping of peripheral blood cells from chimeric animals. M: marker; NC: no template control. (N) ALB (albumin) excretion rate (AER) was measured after 12 weeks of diabetes in transplanted animals. (*$p < 0.05$ DM-WT-c^{WT} vs. ND-WT-c^{WT}; DM-KO-c^{WT} and DM-KO-c^{KO} vs. DM-WT-c^{WT}. (O) Representative images of PAS staining of renal cortex sections from transplanted animals (magnification 400X, scale bar: 50 µm).

Table 3. Metabolic and physiological parameters of chimeric animals.

	ND-WT-c^{WT}	ND-KO-c$^{tnfaip2\ KO}$	DM-WT-c^{WT}	DM-KO-c$^{tnfaip2\ KO}$	DM-KO-c^{WT}
BW (g)	26.02 ± 0.33	26.42 ± 0.51	22.19 ± 0.83[a]	21.77 ± 0.75[a]	22.85 ± 1.52[a]
BG (mg/dl)	124.2 ± 3.64	123.4 ± 3.07	381.0 ± 1.15[b]	397.0 ± 11.70[b]	384.0 ± 34.90[b]
Glycated Hb (%)	4.82 ± 0.19	5.06 ± 0.12	10.48 ± 0.25[b]	10.64 ± 0.26[b]	10.54 ± 0.31[b]
SBP (mmHg)	114.20 ± 5.27	111.20 ± 4.59	108.80 ± 1.15	112.60 ± 1.60	111.4 ± 1.77
KW:BW ratio	5.85 ± 0.01	5.99 ± 0.01	7.29 ± 0.56[c]	7.40 ± 0.10[c]	7.30 ± 0.64[c]
AER (µg/18 h)	19.60 (18.80–19.10)	22.12 (20.20–22.30)	51.46[d] (34.90–66.00)	87.63[e] (77.60–107.90)	84.87[e] (64.30–117.20)

Data are expressed as mean ± SEM or geometric mean (25°-75° percentile); ND; non-diabetic; DM: diabetic; SBP: Systolic Blood Pressure; BW: body weight; BG: blood glucose; KW:BW: kidney weight:body weight; AER: ALB (albumin) Excretion Rate; [a]p<0.05 [b]p<0.001; [c]p<0.01 DM groups vs. ND groups; [d]p<0.05 DM-WT-c^{WT} vs. ND groups; [e]p<0.05 DM-KO-c$^{tnfaip2\ KO}$ and DM-KO-c^{WT} vs. DM-WT-c^{WT}.

injury is required to disclose the renal protective effect of TNFAIP2 in this strain.

Inflammatory mechanisms are important in the pathogenesis of DN [58] and deletion of *Tnfaip2* exacerbated diabetes-induced glomerular inflammation. Moreover, TNFAIP2 is expressed by inflammatory cells and induced by inflammatory cytokines [45,48,50,52]. However, transplantation of BM cells from WT to *tnfaip2* KO mice did not modify the phenotype of recipient diabetic animals. Therefore, lack of *Tnfaip2* in podocytes rather than in inflammatory cells is likely involved in the worsening of experimental DN. Consistently, in diabetic mice TNFAIP2 upregulation occurred predominantly in podocytes and silencing of *Tnfaip2* in isolated cultured podocytes was sufficient to enhance diabetes-induced apoptosis.

In diabetic mice, *tnfaip2* deletion augmented podocyte accumulation of APs by blocking the late stages of the autophagy pathway. Podocytes have a high basal autophagy rate [59,60] and autophagy dysregulation is believed to play an important role in pathogenesis of DN. Consistent with our results in diabetic WT mice, podocyte LC3-II and/or SQSTM1/p62 accumulation have been reported in both human and experimental DN [61–67]. Moreover, disruption of the autophagy-lysosome pathway by AGE-BSA was described in both podocytes and tubular epithelial cells [61,68]. However, changes in autophagy induction are also relevant in experimental diabetes [11,69–71] and both early induction and long-term inhibition of autophagy by hyperglycemia have been shown in mice with STZ-induced diabetes [72]. Moreover, global and podocyte-specific deletion of key regulators of autophagy (*Atg5*, MTOR [mechanistic target of rapamycin kinase] complex 1 [MTORC1], *Sirpa* [signal-regulatory protein alpha]) has been shown to affect susceptibility to DN [65,72–74].

Diabetes-induced alterations in autophagy may also differ in various renal compartments. Our study showed diabetes-induced LC3-II accumulation in both isolated glomeruli and podocytes, while a recent paper demonstrated LC3-II down-regulation in both proximal tubular cells and the renal cortex that consists predominantly of tubules [75]. Opposite effects of diabetes in the glomeruli and the tubules may be due to site-specific differences in autophagy regulation. In line with this, *Mir214* that mediated diabetes-induced LC3-II down-regulation in the tubuli is not expressed by the glomeruli [75]. In addition, tubular cells at variance with podocytes are an active site of glucose reabsorption and this is likely to be relevant in the context of diabetes-induced changes in autophagy. In keeping with this, inhibition of the proximal tubule SLC5A2/SGLT2 (solute carrier family 5 (sodium/glucose cotransporter), member 2) has been shown to ameliorate autophagy deficiency in tubular cells exposed to HG [76].

Altered AP clearance was due to lysosomal dysfunction as proven by worsening of LMP and reduced CTSD activity in diabetes-injured *tnfaip2* KO podocytes. The important role of lysosomes in podocyte injury is increasingly recognised. Mice with podocyte-specific deletion of lysosomal enzymes as *Atp6ap2* (ATPase, H+ transporting, lysosomal accessory protein 2; prorenin receptor) and CTSD show impaired autophagy, podocyte damage, podocyte apoptosis, FP effacement, proteinuria, and renal function loss [77,78]. Moreover, LMP can initiate lysosome-dependent cell death through release of lysosomal content, providing a potential explanation for the enhanced apoptosis of diabetic *tnfaip2* KO podocytes.

Our *in vitro* experiments aimed to clarify the mechanism whereby *Tnfaip2* deficiency enhances lysosomal dysfunction show that *tnfaip2* deletion hampered TNT-mediated transfer among podocytes. Consistent with our previous results [54], we found that podocytes can form TNTs in a TNFAIP2-dependent manner. Several cellular stresses, including oxidative stress, serum deprivation, and hypoxia, have been shown to trigger TNT formation in other cell types [24,33,35,37,38]. Herein, we found that podocyte incubation in a HG milieu induced TNFAIP2 overexpression and that both HG and AGE-BSA were potent TNT inducers. Exposure of mesothelioma cell lines to HG also enhances TNT formation [32]. Moreover, deletion of the AGE receptor *Ager/Rage* (advanced glycosylation end product-specific receptor) has been shown to reduce TNTs in mesothelial cells, astrocytes, and Chinese hamster ovary cells [79,80].

Mechanistically, it has been previously shown that TNFAIP2 cooperates with the RALA/RAL (v-ral simian leukemia viral oncogene A (ras related)) and the exocyst complex to trigger F-actin polymerization and TNT development [45]. The observation that PI3K-AKT1 signaling mediated TNFAIP2 overexpression and TNT formation suggests that the pro-survival effect of the PI3K-AKT1 pathway may be at least in part mediated by induction of the TNFAIP2-TNT system. In line with our results, the AKT1-PI3K pathway has been previously shown to induce *Tnfaip2* mRNA expression in astrocytes [33].

Although TNFAIP2 is required for TNT formation in podocytes and *Tnfaip2* overexpression is known to enhance TNT formation [81], AGEs did not increase TNFAIP2 expression, but still promoted TNT formation. This suggests that induction of TNTs can occur via other mechanisms in

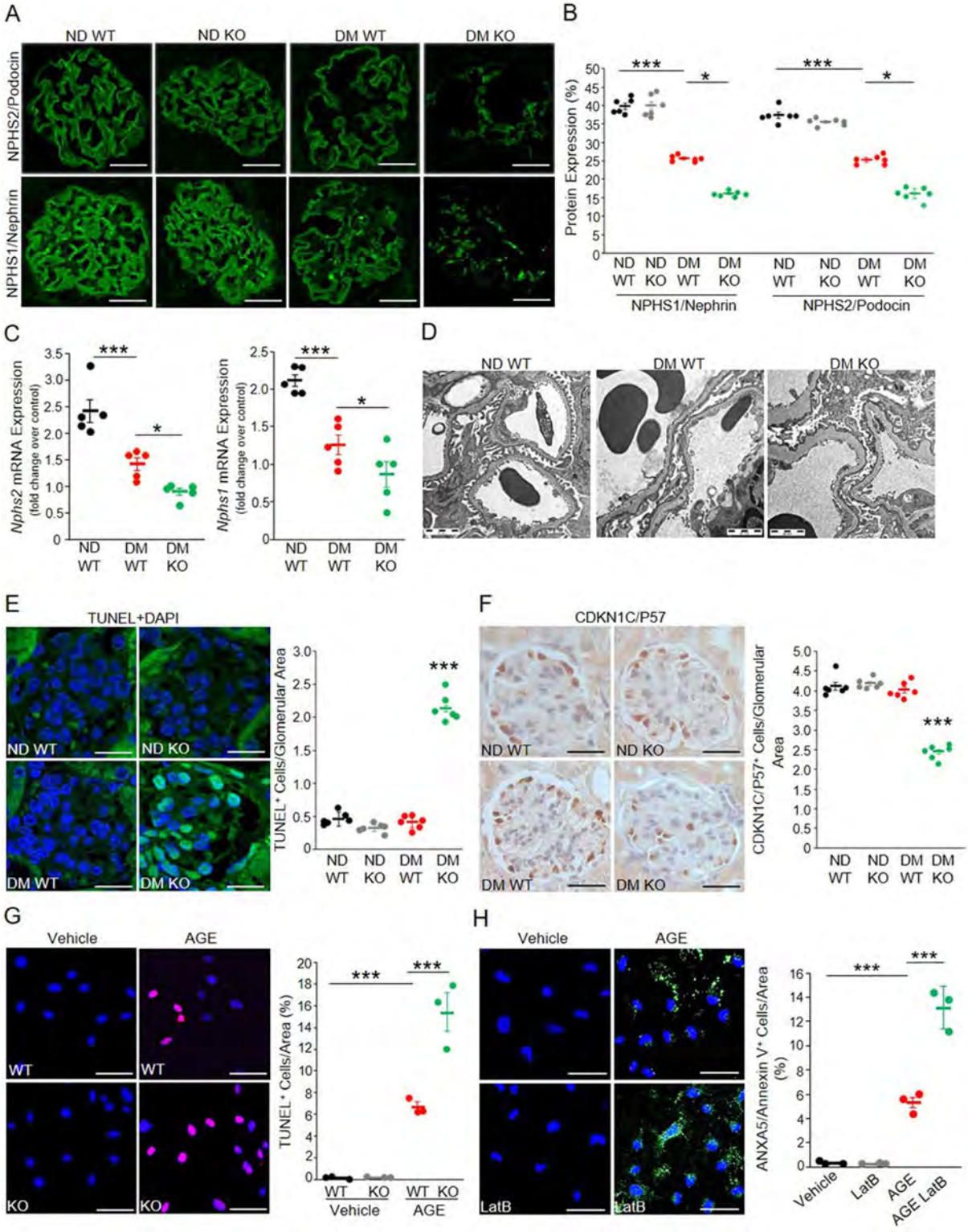

Figure 4. Effect of *tnfaip2* deletion on diabetes-induced podocyte abnormalities. Renal cortex samples from diabetic (DM) and non-diabetic (ND) WT (ND-WT, DM-WT) and *tnfaip2* KO (ND-KO, DM-KO) mice were studied 12 weeks after diabetes onset. (A) Representative immunofluorescence images of NPHS2/Podocin and NPHS1/Nephrin (magnification 400X, scale bar: 50 µm). (B) The graph shows the percent area of NPHS1/Nephrin and NPHS2/Podocin positive staining ($n = 6$ mice per group; ***p < 0.001 DM-WT vs. ND-WT; *p < 0.05 DM-KO vs. DM-WT). (C) *Nphs1* and *Nphs2* mRNA levels were measured by real-time PCR in total renal cortex and the results corrected for the expression of *Wt1* ($n = 5$ mice per group; ***p < 0.001 DM-WT vs. ND-WT; *p < 0.05 DM-KO vs. DM-WT). (D) Electron microscopy images showing glomeruli from ND-WT, DM-WT, and DM-KO mice. The extent of foot processes effacement was greater in DM-KO than in DM-WT animals (magnification 3200X). (E) Apoptosis was assessed by TUNEL assay (green) and nuclei counterstained with DAPI (magnification 400X, scale bar: 50 µm). The percentage of apoptotic cells per glomerular area is shown in the graph ($n = 6$ mice per group; ***p < 0.001 DM-KO vs. others). (F) Representative immunostaining for CDKN1C/P57 (podocyte marker) (magnification 400X, scale bar: 50 µm). The number of CDKN1C/P57-positive cells per glomerular area is reported in the graph ($n = 6$ per group; ***p < 0.001 DM-KO vs. others). (G) Primary podocytes obtained from both WT and *tnfaip2* KO mice were exposed to either vehicle or AGEs for 48 h and apoptosis assessed by TUNEL assay (apoptotic cells in pink). Nuclei were counterstained with DAPI (magnification 100X, scale bar: 200 µm). The percentage of apoptotic cells is shown in the graph (***p < 0.001 WT-AGEs vs. vehicle; KO-AGEs vs. WT-AGEs). (H) Primary podocytes obtained from both WT and *tnfaip2* KO mice were exposed to either vehicle or AGEs for 48 h in the presence/absence of latrunculin-B (LatB, 100 nM) and apoptosis assessed by ANXA5/Annexin V staining (green). Nuclei counterstained with DAPI (magnification 100X, scale bar: 200 µm). The percentage of apoptotic cells is shown in the graph (***p < 0.001 AGEs vs. vehicle; AGEs-LatB. vs. AGEs).

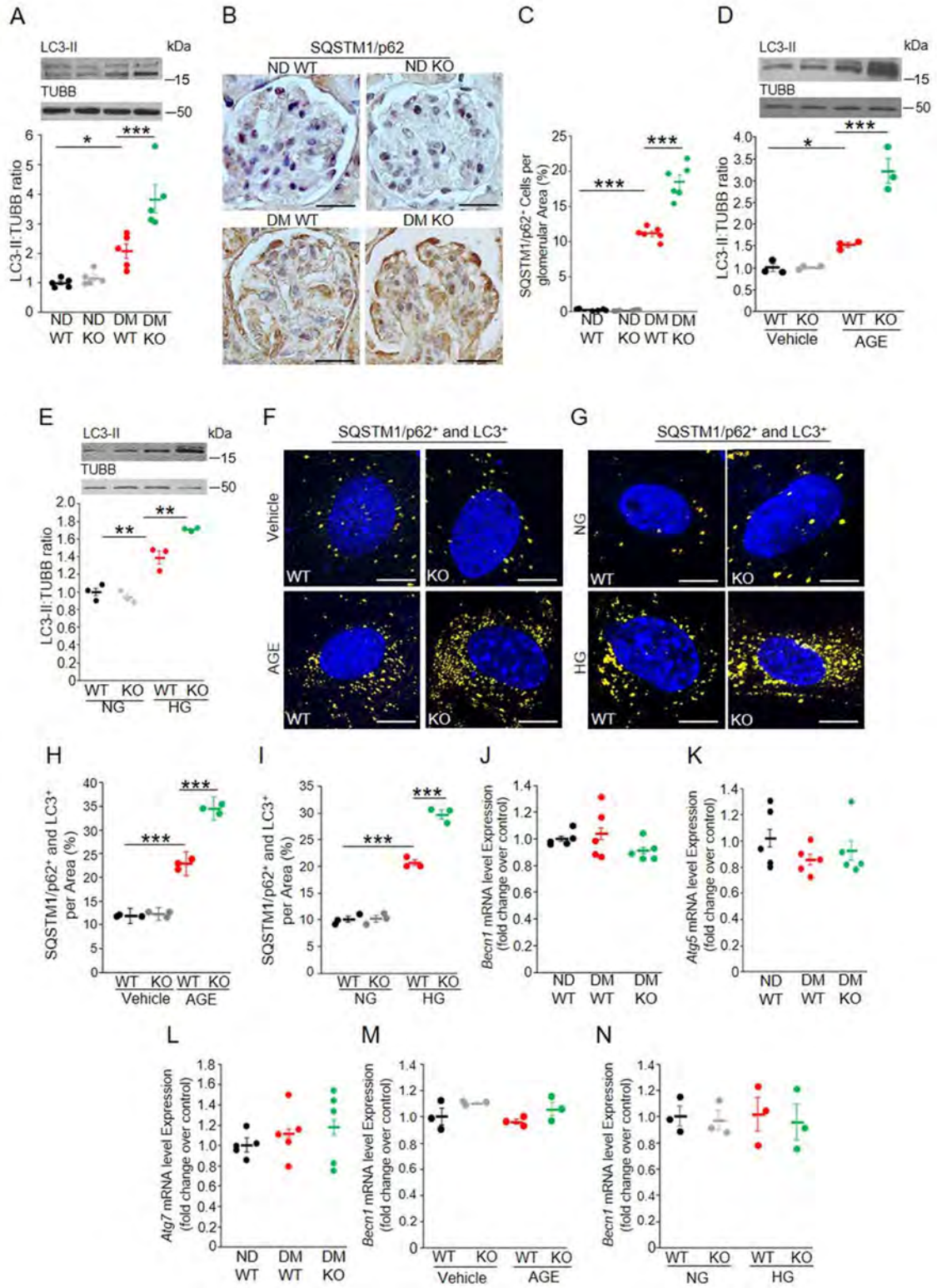

Figure 5. Effect of *tnfaip2* deletion on diabetes-induced autophagy abnormalities. Markers of autophagy were studied in the glomeruli of diabetic and non-diabetic WT (ND-WT, DM-WT) and *tnfaip2* KO (ND-KO, DM-KO) mice and in primary podocytes from ND-WT and ND-KO animals exposed to normal glucose (NG), high glucose (HG), vehicle, or AGEs for 48 h. (A) Immunoblotting showing MAP1LC3/LC3-II expression in isolated glomeruli (TUBB/Tubulin loading control). The graph shows the results of densitometry analysis ($n = 5$ per group; *p < 0.05 DM-WT vs. ND-WT; ***p < 0.001 DM-KO vs. DM-WT). (B) Representative images of glomerular SQSTM1/p62 immunostaining (magnification 400X, scale bar: 50 µm). (C) The graph shows the number of SQSTM1/p62-positive cells per glomerular area ($n = 6$ per group; ***p < 0.001 DM-WT vs. ND-WT; DM-KO vs. DM-WT). (D and E) Immunoblotting showing MAP1LC3/LC3-II expression (TUBB/Tubulin loading control) in cultured podocytes exposed to (D) vehicle or AGEs and (E) NG or HG. Results of densitometry analysis are shown in the graph ($n = 3$; *p < 0.05 WT-AGE vs. vehicle; ***p < 0.001 KO-AGE vs. WT-AGE; **p < 0.01 WT-HG vs. WT-NG and KO-HG). (F and G) Co-staining (yellow dots) for SQSTM1/p62 (green) and MAP1LC3/LC3-II (red) in cultured podocytes exposed to (F) vehicle or AGEs and (G) NG or HG. Nuclei were counterstained with DAPI (magnification X630, bar: 50 µm). (H and I) Quantification of the percent SQSTM1/p62$^+$ and MAP1LC3/LC3$^+$ area is shown in the graphs ($n = 3$; ***p < 0.001 WT-AGE/WT-HG vs. vehicle/NG; KO-AGE/KO-HG vs. WT-AGE/WT-HG). mRNA levels of (J) *Becn1*, (K) *Atg5*, (L) *Atg7* were measured by real time-PCR in the renal cortex of experimental animals and the results corrected for the expression of the housekeeping gene *Hprt* ($n = 5$ per group; p = ns). (M and N) *Becn1* mRNA levels were assessed by real time-PCR in cultured podocytes exposed to (M) vehicle or AGEs, (N) NG or HG. Results were corrected for the expression of the housekeeping gene *Rn18s* ($n = 3$; p = ns).

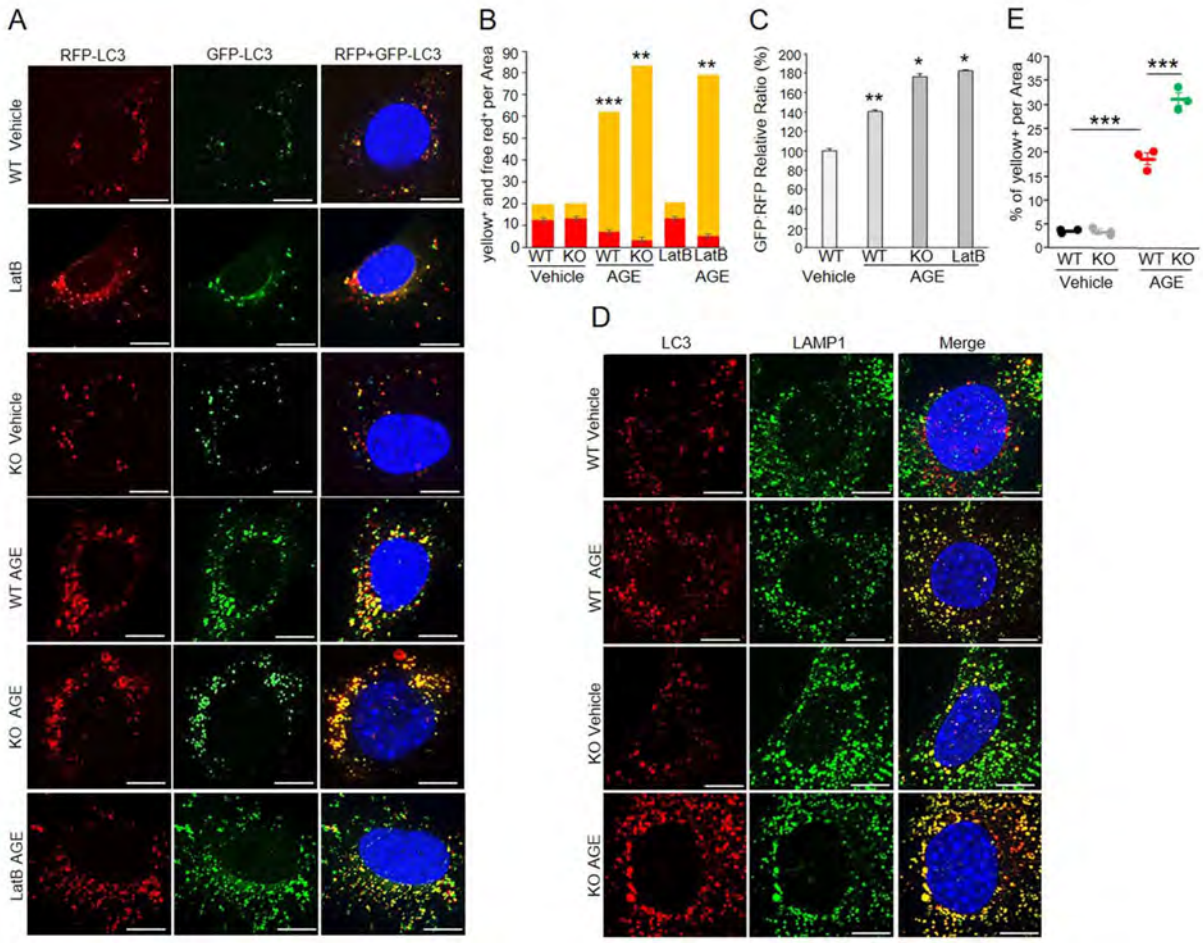

Figure 6. Effect of *tnfaip2* deletion and/or diabetes on both autophagic flux and autolysosome (AL) formation. (A) Autophagy flux was monitored by tandem fluorescent-tagged LC3 in primary WT and *tnfaip2* KO podocytes exposed to either vehicle or AGEs for 48 h in the presence or absence of latrunculin B (LatB). Nuclei were counterstained with DAPI. Yellow puncta autophagosomes (APs) and free red puncta (acidic AL) are shown in the RFP+GFP-LC3 panels (magnification X630, bar: 50 µm). (B) Quantification of the number of yellow and free red puncta per cell is shown in the graph ($n = 3$; ***p < 0.001 WT-AGE vs. vehicle; **p < 0.01 KO-AGE and LatB-AGE vs. WT-AGE). (C) The relative GFP:RFP ratio was assessed by ImageJ and results are shown in the graph (**p < 0.01 WT-AGE vs. vehicle; *p < 0.05 KO-AGE and LatB-AGE vs. WT-AGE). (D) Fusion of APs with lysosomes was assessed by double immunofluorescence for MAPLC3/LC3 (red) and LAMP1 (green). Merged images showed co-localization (magnification X630, bar: 50 µm). (E) The graph shows the percentage of the yellow positive area per cell (***p < 0.001 WT-AGE vs. WT-vehicle; KO-AGE vs. WT-AGE).

addition to TNFAIP2 overexpression, though the presence of TNFAIP2 is still required for this to take place. Factors, inducing actin remodeling, which orchestrates TNT formation, are likely candidates.

As hyperglycemia, AGEs, and consequent oxidative stress/inflammation are stressful conditions to cells, it is not surprising that they induce TNT formation. Indeed, the ability of cells to interconnect and to share a common pool of resources via TNTs represents a potent rescue mechanism that provides significant survival advantages by allowing individual cells as part of a supercellular system to maintain redox and metabolic homeostasis [82].

TNTs interconnecting podocytes transferred lysosomes in a TNFAIP2 dependent manner. Lysosome transport from healthy to AGE-injured podocytes was enhanced, suggesting that it was aimed to rescue podocytes with dysfunctional lysosomes by delivering healthy organelles. Transfer of APs in the opposite direction was also observed and may represent a mechanism to dilute the overload of dysfunctional APs among cells, thus preventing extreme organelle dysfunction [82]. Notably, lysosome transfer was also seen when donor and recipient podocytes were pre-exposed to different AGE-BSA concentrations to mimic the *in vivo* condition in which podocytes are all exposed to the diabetes insult, but may have different degrees of lysosomal dysfunction.

Lysosome transfer via TNTs has been previously demonstrated in other cell types [43,83–86]. Moreover, TNT-mediated lysosomal transfer has been shown to correct cystinosis, a genetic lysosomal disease, through bidirectional lysosome exchange between hematopoietic stem cells (HSC)-derived macrophages and cystinosin-deficient cells [87]. However, lysosome transfer can also be deleterious and it has been implicated in the spreading of neurotoxic aggregates in neurodegenerative diseases [88]. Evidence of AP transfer is more limited; however, AP shuttling via TNTs has been reported in both squamous cell carcinoma [44] and the leukemic niche [89].

Deficiency of *Tnfaip2* may enhance diabetes-induced accumulation of damaged APs and lysosomes, possibly

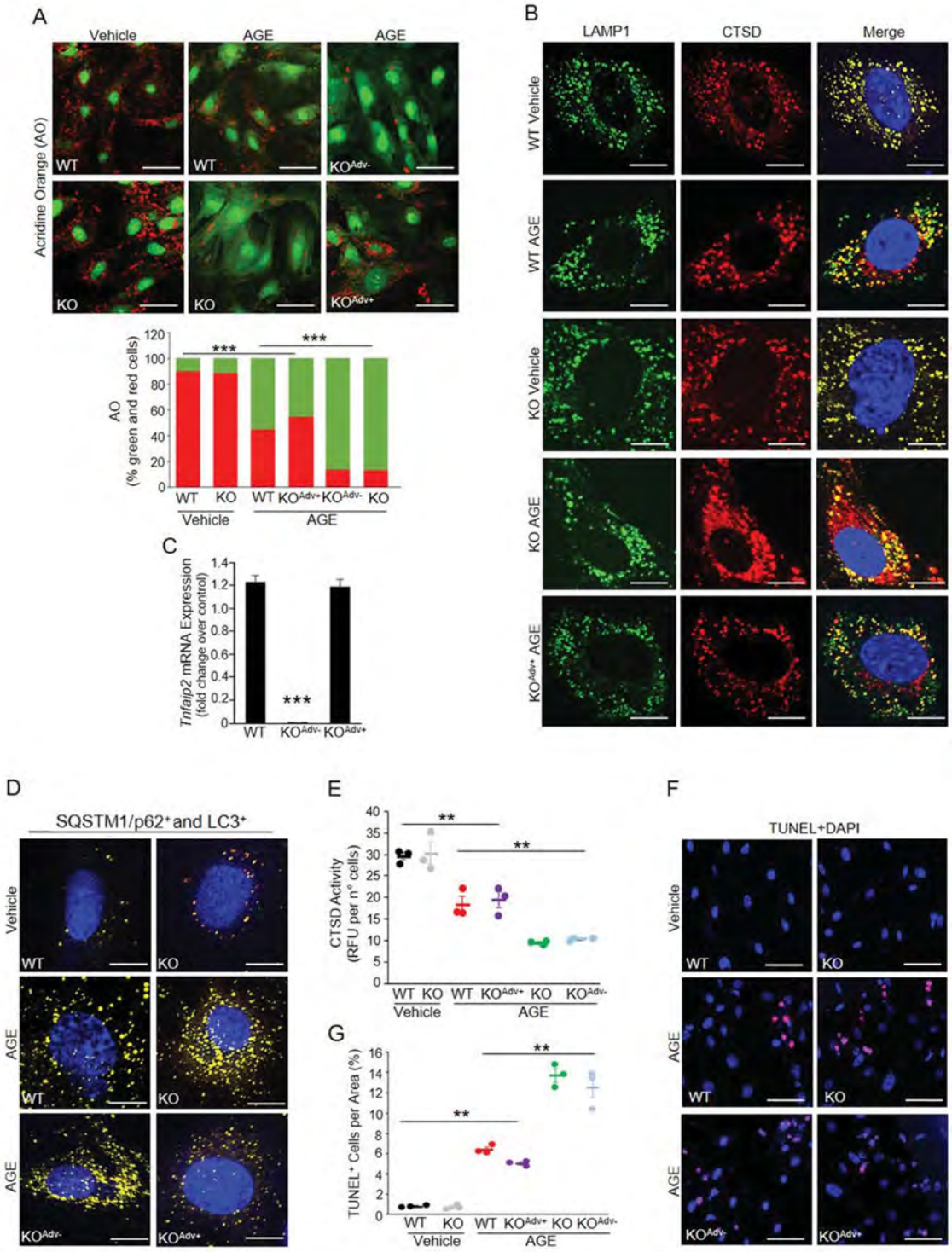

Figure 7. Effect of *tnfaip2* deletion and re-expression on diabetes-induced changes on lysosomes, autophagosomes (APs), and apoptosis. Lysosome both integrity and function was assessed in primary murine WT and *tnfaip2* KO podocytes exposed to either vehicle or AGEs for 48 h. The effect of *tnfaip2* re-expression on lysosomal integrity and function, AP accumulation, and apoptosis was tested by transfecting KO podocytes with an adenovirus expressing either *Tnfaip2* (KO^{Adv+}) or a control mock vector (KO^{Adv-}). (A) Representative immunofluorescence images of podocytes stained with Acridine Orange (AO) (magnification X100, bar: 200 µm). Quantification of green to red AO fluorescence is reported in the graph below ($n = 3$; ***$p < 0.001$ WT-AGE and KO^{Adv+}-AGE vs. WT-vehicle; KO-AGE and KO^{Adv-}AGE vs. WT-AGE). (B) Colocalization of CTSD (red) with $LAMP1^+$ lysosomes (green). Nuclei were stained with DAPI (magnification X630, bar: 50 µm). (C) *Tnfaip2* mRNA levels were measured by real-time PCR in WT, KO^{Adv+} and KO^{Adv-} podocytes and the results corrected for the expression of *Rn18s* ($n = 3$; ***$p < 0.001$ KO^{Adv-} vs. others). (D) Effect of *Tnfaip2* re-expression on AP accumulation as shown by costaining (yellow dots) for SQSTM1/p62 (green) and MAP1LC3/LC3 (red). Nuclei were counterstained with DAPI (magnification X630, bar: 50 µm). (E) Quantification of CTSD activity expressed as relative fluorescence units (RFU) per number of cells (**$p < 0.01$ WT-AGE and KO^{Adv+}-AGE vs. WT-vehicle; KO-AGE and KO^{Adv-}AGE vs. WT-AGE). (F) Effect of *Tnfaip2* re-expression on podocyte apoptosis assessed by TUNEL assay (apoptotic cells in pink) (magnification 100X, scale bar: 200 µm). (G) The percentage of apoptotic cells is shown in the graph (**$p < 0.01$ WT-AGE and KO^{Adv+}-AGE vs. WT-vehicle; KO-AGE and KO^{Adv-}AGE vs. WT-AGE).

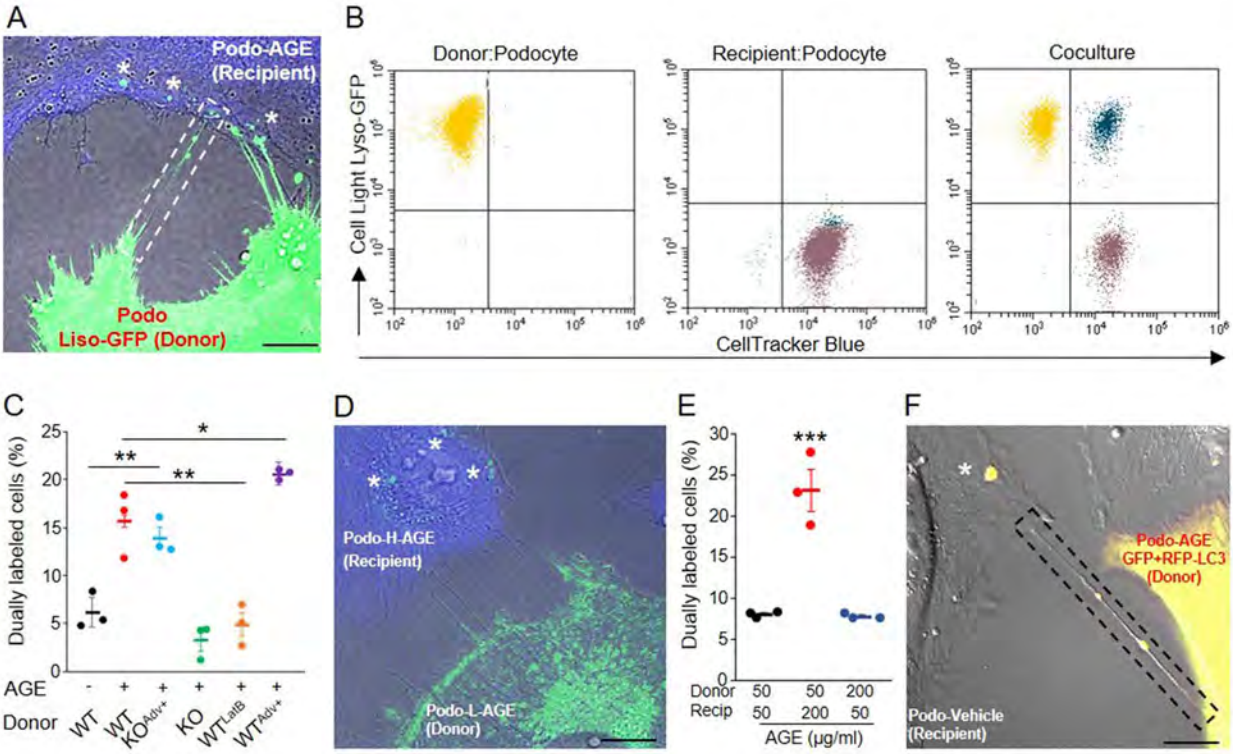

Figure 8. TNFAIP2-TNT-mediated lysosome and autophagosome (AP) exchange in AGE-treated podocytes. (A) Podocytes stained with CellTracker Blue were exposed to either vehicle or AGEs for 48 h, and then cocultured with donor podocytes carrying LAMP1-GFP-labeled lysosomes. The images show green lysosomes within the TNT and in the cytosol (*) of a recipient podocyte (magnification X630, bar: 50 μm, DIC images showing the TNT). (B and C) Lysosome transfer (GFP and Blue dually labeled cells) was quantified by flow cytometry in recipient podocytes exposed to either vehicle or AGEs and co-cultured with donor WT and *tnfaip2* KO podocytes. WT donor podocytes were treated with latrunculin-B (WT-LatB 100 nM, 1 h) to prevent TNT formation. KO and WT donor podocytes were transfected with an adenovirus expressing either *tnfaip2* (KO^{Adv+}, WT^{Adv+}) or a mock vector ($n = 3$; **$p < 0.01$ WT-AGE and KO^{Adv+}-AGE vs. WT-Vehicle; KO-AGE, WT^{LatB}-AGE vs. WT-AGE; $p < 0.05$ WT^{Adv+}-AGE vs. WT-AGE). (D) Recipient podocytes were stained with CellTracker Blue and exposed to high AGE concentration (200 μg/ml, 48 h; H-AGE). Donor podocytes with LAMP1-GFP-labeled lysosomes were exposed to lower AGE concentrations (50 μg/ml, 48 h; L-AGE). In coculture, green lysosomes were seen in the cytosol (*) of recipient podocytes (magnification X630, bar: 50 μm, DIC images showing the TNT). (E) Donor (GFP-labeled lysosomes) and recipient (Recip, CellTracker Blue) podocytes were pre-exposed to either H-AGE (200 μg/ml) or L-AGE (50 μg/ml) concentrations and then co-cultured. Lysosome transfer (GFP and Blue dually labeled cells) from donor towards recipient (Recip) podocytes was quantified by flow cytometry (***$p < 0.001$ Donor-L-AGE to Recip-H-AGE vs. others). (F) Donor podocytes exposed to AGEs for 48 h were transfected with tandem fluorescent-tagged LC3 to label APs (yellow punta), then co-cultured with healthy recipient podocytes. The image shows yellow puncta within the TNT and in the cytosol (*) of a recipient podocyte (magnification X630, bar: 50 μm, DIC images showing the TNT).

explaining worsening of DN in *tnfaip2* KO mice. In keeping with this hypothesis, TNFAIP2-TNT-mediated transfer from healthy to AGE-BSA-exposed podocytes ameliorated autophagy, lysosome dysfunction, and apoptosis in recipient cells.

We cannot exclude the possibility that transfer of other organelles was also implicated as TNTs have been shown to transport mitochondria, mRNA, lipid droplets, virus, vesicles in other cell types and mitochondria in podocytes. However, donor podocytes carrying altered lysosomes failed to improve autophagy, lysosome dysfunction, and podocyte apoptosis, suggesting that TNFAIP2 protected podocytes predominantly through TNT-mediated lysosome transfer.

Importantly, overexpression of *Tnfaip2* in donor podocytes enhanced lysosome transfer towards podocytes exposed to AGE-BSA and almost abolished the deleterious effect of AGE-BSA on autophagy, lysosome function, and apoptosis in recipient cells. A similar cytoprotective effect of *Tnfaip2* overexpression was also observed in monoculture of podocytes exposed to AGE-BSA, a model that more closely resembles the *in vivo* condition. Therefore, lack of the TNFAIP2-TNT system worsened diabetes-induced podocyte injury, while its induction counteracted the deleterious effects of diabetes.

In conclusion, we demonstrated that the TNFAIP2-TNT system has an important protective role in DN. As several cell types express this system, our findings may also be relevant to other diabetes complications. Evidence that diabetes-injured podocytes can be rescued by *Tnfaip2* overexpression suggests that the TNFAIP2-TNT system may represent a novel druggable target.

Materials and methods

Patients

Archival Serra's fluid-fixed, paraffin-embedded kidney sections from patients with type 2 diabetes with either incipient ($n = 3$, 30–300 mg/24 h) or overt nephropathy ($n = 12$, persistent proteinuria >0.5 g/24 h) were studies. Renal tissue from subjects (n = 8), who underwent surgery for localized grade I hypernephroma and did not have proteinuria or glomerular abnormalities, as detected by both light and immunofluorescence microscopy, was used as control. Proteinuria was

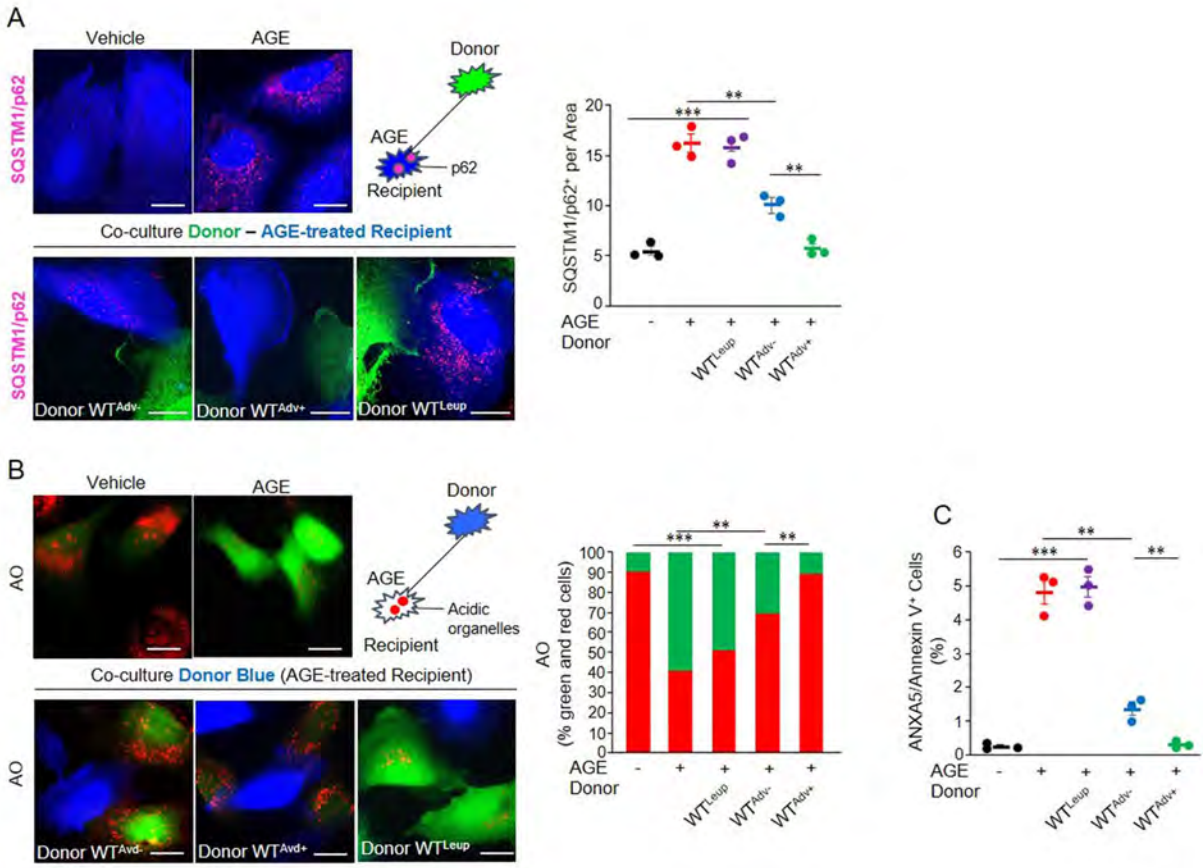

Figure 9. Effect of TNFAIP2-TNT-mediated lysosome exchange on autophagosome (AP) accumulation, lysosome dysfunction, and apoptosis in a co-culture system. Podocytes were exposed to either vehicle or AGEs for 48 h. The effect of the TNFAIP2-TNT system on autophagy, lysosome dysfunction, and apoptosis was assessed by co-culturing recipient AGE-treated podocytes with donor (D) cells transfected with an adenovirus expressing *Tnfaip2* (WT^{Adv+}), mock vector (WT^{Adv-}) or pre-exposed to leupeptin (Leup, 200 µg/ml WT^{Leup}). (A) Immunostaining for SQSTM1/p62 (pink). Blue recipient podocyte (CellTracker Blue) and green donor podocytes (CellTracker Green) (magnification 630X, scale bar: 50 µm) and quantification of $SQSTM1/p62^{+}$ positive area per cell ($n = 3$; ***p < 0.001 AGE and AGE+Donor-WT^{Leup} vs. vehicle; **p < 0.01 AGE-Donor-WT^{Adv-} vs. AGE andAGE-Donor-WT^{Adv+}). (B) Acridine Orange (AO red and green) staining. Blue donor podocytes (CellTracker Blue) (magnification 630X, scale bar: 50 µm) and quantification of green to red AO fluorescence ($n = 3$; ***p < 0.001 AGE and AGE+Donor-WT^{Leup} vs. vehicle; **p < 0.01 AGE-Donor-WT^{Adv-} vs. AGE and AGE-Donor-WT^{Adv+}). (C) The graph shows the percentage of apoptotic podocytes as assessed by ANXA5/Annexin V staining ($n = 3$; ***p < 0.001 AGE and AGE+Donor-WT^{Leup} vs. vehicle; **p < 0.01 AGE-Donor-WT^{Adv-} vs. AGE and AGE-Donor-WT^{Adv+}).

measured by Pyrogallol-red on three separate urine collections and serum creatinine by the kinetic Jaffè method on a Beckman Synchron CX3 analyser (Beckman Coulter, Italy). Hypertension was defined for blood pressure values >140/90 mmHg measured in three separate occasions [90]. All clinical procedures were in accordance with the Helsinki Declaration.

Mice

Male C57BL/6 mice were purchased from Charles River Laboratories (Milan, Italy). The *tfnaip2* KO C57BL/6 mice were generated at the Riken Center in Japan, as we have previously reported [54]. Animals were maintained on a normal diet and both housing and care of laboratory animals were in accordance with Italian law. Procedures were approved by the Ethical Committee of the Turin University, Italy.

Diabetes induction

Diabetes was induced in 8-week-old both WT and *tnfaip2* KO C57BL/6 mice by STZ intraperitoneal injection (Merck Life Science, S0130; 55 mg/Kg for 5 consecutive days). Control mice were injected with sodium citrate buffer. Diabetes onset was confirmed by blood glucose levels >250 mg/dl four weeks after the first dose of STZ. Before sacrifice, blood samples were taken via saphenous vein puncture on alert, 4 h–fasted animals, and glucose levels measured using a glucometer (Accu-chek Aviva, Italy). Systolic blood pressure was measured by tail-cuff plethysmography. Urine was collected over 18 h, with each mouse individually housed in a metabolic cage and provided with food and water *ad libitum*. Urinary ALB concentration was measured by a mouse albumin ELISA kit (Bethyl Laboratories, E99-134). Creatinine clearance was calculated from urine and serum creatinine concentrations, as determined by high-performance liquid chromatography (HPLC) [91]. Glycated hemoglobin was measured by quantitative immunoturbidimetric latex determination (Sentinel Diagnostic, 17,418). Twelve weeks after diabetes onset, mice were euthanized, and kidneys removed and weighted; half a kidney was formalin-fixed and paraffin-embedded for light microscopy analyses and the other half was included in optimal cutting temperature compound (VWR, 00411243) and snap-frozen in N_2. The other kidney was stored at −80°C for RNA and protein analyses. In a subset

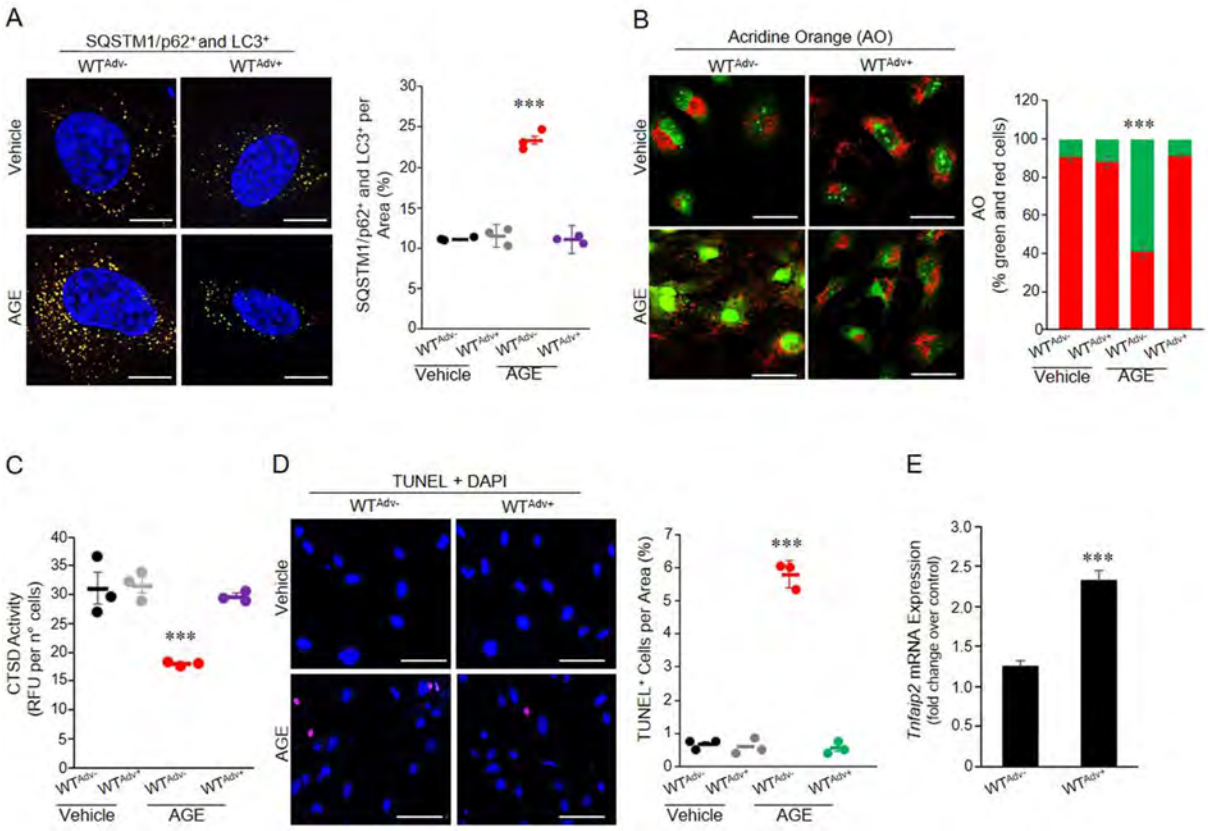

Figure 10. Effect of *Tnfaip2* over-expression in monoculture of AGE-treated podocytes. WT podocytes and podocytes transfected with an adenovirus expressing *Tnfaip2* (WT^{Adv+}) or a mock vector (WT^{Adv-}) were exposed to either vehicle or AGEs for 48 h. (A) Double immunostaining (yellow dots-autophagosomes) for MAP1LC3/$LC3^+$ and SQSTM1/$p62^+$ (magnification X630, bar: 50 µm, nuclei: DAPI) and quantification of the percent SQSTM1/$p62^+$ and MAP1LC3/$LC3^+$ positive area (n = 3; ***p < 0.001 AGE-WT^{Adv-} vs. others). (B) Acridine Orange (AO) staining (magnification 100X, scale bar: 200 µm) and quantification of green and red AO fluorescence (n = 3; ***p < 0.001 AGE-WT^{Adv-} vs. others). (C) CTSD activity expressed as relative fluorescence units (RFU) per number of cells (n = 3; ***p < 0.001 AGE-WT^{Adv-} vs. others). (D) Images of apoptotic podocytes (pink, TUNEL assay) (magnification 100X, scale bar: 200 µm, nuclei: DAPI) and quantification of the percentage of TUNEL positive cells (n = 3; ***p < 0.001 AGE-WT^{Adv-} vs. others). (E) *Tnfaip2* mRNA levels were measured by real-time PCR in WT^{Adv+} and WT^{Adv-} podocytes and the results corrected for the expression of *Rn18s* (n = 3; ***p < 0.001 WT^{Adv+} vs. WT^{Adv+}).

of mice, glomeruli were isolated using a modified Dynabead method, as previously described, at both 6 and 12 weeks after diabetes induction [54].

Chimeric mice

Eight-week-old male WT and *tnfaip2* KO mice were used as BM donors. BM cells were flushed from tibial and femoral cavities under sterile conditions, filtered through 70 µm nylon meshes (Corning, 431,751), and then transplanted without further purification or *in vitro* expansion. Recipient male mice, aged 8 weeks, underwent whole body-irradiation (8 Gy) and 24 h later injected with 2.0×10^6 BM cells via the tail vein. The *tnfaip2* KO mice received a BM transplant from either WT (KO-c^{WT}; n = 5) or *tnfaip2* KO (KO-c^{KO}; n = 5) animals and WT recipients from WT animals (*WT*-c^{WT}; n = 5). DNA was isolated from blood cells (Thermo Fisher Scientific, K1820-02) and chimerism confirmed by polymerase chain reaction (PCR).

Podocytes

Primary podocytes were obtained from both six-week-old C57BL/6 WT and *tnfaip2* KO mice, as previously described. Briefly, decapsulated kidneys were digested in 1 mg/ml collagenase A (Merck Life Science, C9407) for 30 min at 37°C. Glomeruli were isolated using Dynabeads (Thermo Fisher Scientific, 14,013) and cultured for 4–5 days on type IV collagen (Merck Life Science, C5533)-coated dishes, in DMEM medium (Gibco, 31,885–023) supplemented with 10% fetal bovine serum (Gibco, 10,270–106), 100 U/ml penicillin/100 and µg/ml streptomycin (Gibco, 15,070–063), 2 mM L-glutamine (Gibco, 25,030–024), 100 mM 4-(2-hydroxyethyl)-1-piperazineethanesulfonic acid (HEPES; Merck Life Science, H3375). Subculture of primary podocytes was performed by detaching glomerular cells with trypsin-ethylenediaminetetraacetic acid (EDTA; Merck Life Science, T4174) followed by sieving through 30-µm pore cell strainers (PluriSelect, 43–50,030-01). For TNT visualization, organelle transfer detection, and immunofluorescence staining, podocytes were seeded onto 35-mm µ-dishes (Ibidi, 80,136; 60,000 cells per dish). Cells were exposed either to HG (25 mM) or NG (7 mM made iso-osmolar with mannitol [Merck Life Science, M1902]), AGE-BSA/BSA (Merck Life Science, 121,800-M; 50, 100, and 200 µg/ml) for 48 h. In 24 h-mechanical stretch experiments, cells were seeded on type I collagen-coated silicon elastomer-base culture plates (Flexcell

International, BF-3001C) and connected to a vacuum pump to result in a 10% elongation; control cells were grown in non-deformable, but otherwise identical plates.

In some experiments, cells were pre-incubated with 100 nM latrunculin B (Merck Life Science, L5288), 1 μM AKT1 inhibitor VIII (Merck Life Science, 124,018), 50 μM LY294002 (Merck Life Science, L9908), 5 μM p-nitro-Pifithrin -α (Santa Cruz Biotechnology, sc222176), or 200 μg/ml leupeptin (Merck Life Science, L2884).

To knockdown *Tfnaip2*, podocytes (3 x 10^5 cells) were transfected using Lipofectamine 3000 Transfection Reagent (Thermo Fisher Scientific, L3000001) with a plasmid construct encoding *Tnfaip2*-specific sh-RNA (shRNA: *5'-GGCAATCTACCA AGCAGTGAAGTCAGGAG-3'*, scramble negative control: *5' GCACTACCAGAGCTAACTCAGATAGTACT 3'*) cloned in a pRS vector (ExactHuSH, OriGene Technologies Inc, TL513846). To overexpress *Tnfaip2*, cells were transfected with a mouse *Tnfaip2* adenovirus (Vectors Biolabs, AAV-274678). Western blotting was performed to assess the knockdown/overexpression efficiency.

TNTs and organelle transfer

To reveal TNTs, podocytes were labeled with Alexa Fluor®-488 conjugated-wheat germ agglutinin (WGA; Thermo Fisher Scientific, W11261; 5 μg/ml) and imaged by Apotome II Zeiss Microscope controlled by Axiovision software with 0.25-μm Z-stacks. After image acquisition, the number of cells connected by WGA-labeled straight structures that did not adhere to the substrate, as assessed by Z-stack, and were thinner than 1 μm was counted in blind. Data were presented as the percentage of total counted cells (at least 200 cells).

In transfer experiments, recipient podocytes were labeled with the cytoplasmic dye Cell Tracker Blue CMFDA (Thermo Fisher Scientific, C2110; 5 μM). Donor podocytes were transfected with a modified insect virus (Baculovirus) expressing a fusion construct of a green fluorescent protein with the lysosomal protein LAMP1 (Cell Light™ Lysosomes-GFP BacMam 2.0; Thermo Fisher Scientific, C10596). Cells were co-cultured at a ratio of 1:1 for 24 h. To visually assess lysosome transfer, both fluorescent and differential interference contrast (DIC) microscopy were used. To quantify lysosomal transfer efficiency, cells were fixed in 2% w:v paraformaldehyde (PFA; Merck Life Science, 158,127), passed through a cell strainer, then analyzed by flow cytometry (Citoflex, Beckman Coulter, USA). Single positive cells (donor and recipient cells alone) were used to set up the instrument. Data analysis was performed using the Cytexpert software (Version 2.3). To control for TNT-independent transfer, recipient cells were plated in the bottom compartment of a transwell system (Corning, 3401) and donor cells on a 0.4-μm pore-sized insert.

Autophagy, lysosome dysfunction, and apoptosis

Autophagic flux was assessed in podocytes transfected with Premo™ Autophagy Tandem Sensor RFP-GFP-LC3B (Thermo Fisher Scientific, P36239). Results were expressed as the number of yellow and free red puncta per cell as well as relative GFP:RFP ratio (at least 50 cells). CTSD enzymatic activity was measured using a fluorescence-based assay kit (BioVision, K143-100) and results expressed as relative fluorescence units (RFU) per number of cells. For acidic organelle labeling, cells were incubated with 1 μg/ml of AO (Thermo Fisher Scientific, A1301) for 10 min, washed with phosphate-buffered saline (PBS; Merck Life Science, 79,382), and then fixed in 100% methanol. Results were expressed as green to red AO fluorescence (at least 100 cells). Apoptosis was detected by either transferase-mediated dUTP nick end-labeling (TUNEL) assay (Millipore, S7165) or Alexa Fluor® 488-conjugated ANXA5/annexin V (Thermo Fisher Scientific, A13201). Results were expressed as the percentage of apoptotic (TUNEL or ANXA5-positive cells) per glomerular or cellular area.

Microscopy

Light microscopy

Paraffin-embedded renal sections were stained using PAS. The mesangial index (mesangial area:total area of glomerulus) was quantified with Axiovision software (Zeiss, Germany; Version 4.7) in 15 glomeruli per kidney per animal.

Electron microscopy

Renal cortex pieces (1 mm^3) were fixed in 2% glutaraldehyde (Merck Life Science, G7651), 4% PFA in PBS for 4 h at room temperature. Samples were then postfixed in 1% osmium tetroxide (Merck Life Science, 201,030) for 2 h, dehydrated, and embedded in Epon 812 (Fisher Scientific, 50,980,391). Ultrathin sections (70 nm) were cut using a Leica EM UC6 ultramicrotome, counterstained with uranyl acetate and lead citrate, and analyzed with an Energy Filter Transmission Electron Microscope (EFTEM, ZEISS LIBRA® 120, Germany) equipped with an yttrium aluminum garnet scintillator slow-scan charge-coupled device camera (Sharp eye, TRS, Moorenweis, Germany). Analysis was performed blindly in 10 glomeruli for each animal.

Fluorescence and DIC microscopy

A Zeiss APOTOME 2 system (Zeiss, Germany) equipped with an incubator for live-cell imaging microscopy and Nomarski optics for DIC microscopy was used in TNT studies. DIC microscopy was used to avoid TNT phototoxic damage. Sequences of optical planes (Z-stack) were acquired for reconstruction in the x-z plane.

mRNA analysis

Total RNA was extracted using the TRIZOL reagent (Thermo Fisher Scientific, 15,596,026). One or two μg of total RNA was reverse transcribed into cDNA using the high-capacity cDNA reverse transcription kit (Thermo Fisher Scientific, 4,368,814). mRNA expression was assessed by real-time PCR using the TaqMan Gene Expression Master Mix (Thermo Fisher Scientific, 4,369,016), and the pre-developed TaqMan primer/probes: *Tnfaip2* (Mm00447578), *Nphs1* (Mm00497828), *Nphs2*

(Mm00499929), *Tgfb1* (Mm00441724), *Ly6c2* (Mm00841873), *Ccl2* (Mm00441242), *Ccr2* (Mm00438270), *Tnf* (Mm00443258), *Becn1* (Mm01265461), *Atg5* (Mm01187303), *Atg7* (Mm00512209) (Thermo Fisher Scientific). Amplification was performed using the Abi Prism 7300 (Thermo Fisher Scientific, Italy). Relative quantification was carried out using the $2^{-\Delta\Delta Ct}$ method using either *Hprt* (hypoxanthine guanine phosphoribosyl transferase; Mm00446968) or *Wt1* (Mm00460570) or *Rn18s* (Thermo Fisher Scientific, 4,333,760 T) as endogenous controls.

Protein Analysis

Renal cortex sections. immunohistochemistry (IHC) and double immunofluorescence (D-IF)

After antigen retrieval and blocking in 3% BSA (Merck Life Science, A6003), 4-µm kidney paraffin sections were incubated overnight at 4°C with the following primary antibodies: rabbit anti-TNFAIP2 (Abcam, ab196659; 1:100), rabbit anti-NPHS2/podocin (Merck Life Science, P0372; 1:200), rat-anti LGALS3/MAC2 (Cederlane, CL8942AP; 1:100), rabbit anti-CDKN1C/P57 (Santa Cruz Biotechnology, sc-8298; 1:100), rabbit anti-SQSTM1/p62 (Abcam, ab91526; 1:100). After washing, sections were incubated with goat anti-rat (Jackson ImmunoResearch Laboratories, 112–065-003; 1:500) or swine-anti rabbit (DAKO, E0353; 1:200) biotinylated secondary antibodies for 1 h.

For IHC, sections were then incubated with horseradish peroxidase (HRP)-conjugated streptavidin (DAKO, P0397; 1:300) for 1 h. Diaminobenzidine (Merck Life Science, D5905) was used as a chromogen substrate for HRP. Sections were visualized with an Olympus-BX4I microscope and digitized with a high-resolution camera (Zeiss, Germany). On average 30 randomly selected glomeruli were assessed per mouse. Results are expressed either as the number of positive cells per glomerular area or as percent area of positive staining per glomerulus. Two investigators performed evaluations in a blinded fashion.

For D-IF on human biopsies, sections were then incubated with Alexa Fluor 488-conjugated streptavidin (Thermo Fisher Scientific, S11223; 1:100). After further blocking in BSA, sections were incubated with an anti-mouse SYNPO (Progen, 61,094; 1:50) antibody for 18 h at 4°C, followed by RPE-conjugated goat anti-mouse (DAKO, R0480; 1:50). Digitized images were color-combined and assembled into photomontages by using Adobe Photoshop (Universal Imaging Corporation).

Immunofluorescence (IF). renal cortex

Single-antigen IF on mouse tissue was performed on snap-frozen kidney sections (3 µm). Slides were fixed in acetone for 5 min and blocked in 3% BSA, then incubated overnight at 4°C with guinea pig anti-NPHS1/Nephrin (Progen, GP-N2; 1:100), rabbit anti-NPHS2/Podocin, or rabbit anti-FN1 /Fibronectin (Merck Life Science, F3648; 1:200) primary antibodies. Following washing, fluorescein isothiocyanate (FITC)-conjugated goat anti-guinea pig (Santa Cruz Biotechnology, sc-2441; 1:50) or swine anti-rabbit (DAKO, F0205; 1:50) secondary antibodies were incubated for 1 h. Sections were examined using a Zeiss APOTOME 2 system equipped with a high-resolution camera (Zeiss, Germany) and quantitated using the Axiovision 4.7 image analysis software (Zeiss, Germany). Results were expressed as the percentage of positively stained tissue within the glomerular tuft. On average 20 randomly selected hilar glomerular tuft cross-sections were assessed per mouse.

Cultured cell

Podocytes were fixed in 4% w:v PFA for 15 min. To avoid disruption of existing TNTs during fixation, 16% w:v PFA was added along the sides of the plates, keeping the overlying culture medium intact, to a final w:v concentration of 4%. Cells were then permeabilized using 0.5% v:v Triton X-100 (Merck Life Science, 9002–93-1) for 5 min at 4°C. Cultures were then blocked with 3% BSA and incubated overnight at 4°C with a mouse anti-SQSTM1/p62 (Santa Cruz Biotechnology, sc-48,402; 1:100) or rat anti-LAMP1 (Santa Cruz Biotechnology, sc-19,992; 1:100) primary antibody. After washing, FITC-conjugated goat anti-mouse (Thermo Fisher Scientific, A16079; 1:50) or goat anti-rat (Merck Life Science, F6258; 1:50) secondary antibodies were added for 1 h. FITC-SQSTM1/p62 labeled cells were, then, incubated overnight at 4°C with a rabbit anti-MAP1LC3/LC3 (Cell Signaling Technology, 43,566; 1:100) followed by incubation with tetramethylrhodamine (TRITC)-conjugated pig anti-rabbit (DAKO, R0156; 1:50). FITC-LAMP1-labeled cells were incubated for 1 h at room temperature with either a rabbit anti-MAP1LC3/LC3 or a goat anti-CTSD (R&D Systems, AF1029; 1:100) antibody, followed by incubation with TRITC-conjugated pig anti-rabbit or Alexa Fluor® 555-conjugated donkey anti-goat (Thermo Fisher Scientific, A21432; 1:1000) antibodies, respectively. Cell nuclei were counterstained with a 4′,6-diamidino-2-phenylindole (DAPI) solution. Digitalised images were color-combined and assembled into photomontages by using Adobe Photoshop (Universal Imaging Corporation).

Immunoblotting

Equal amounts of protein samples were separated on sodium dodecyl sulfate (SDS)-polyacrylamide gel electrophoresis and electro-transferred to nitrocellulose membranes. Following blocking, membranes were incubated with anti-TNFAIP2 or anti-MAP1LC3/LC3 primary antibodies overnight at 4°C. After washing, secondary HRP-linked antibodies (GE Healthcare, RPN4301; 1:10,000) were added for 1 h. Detection was performed using Super signal PICO (Thermo Fisher scientific, 34,580) and visualized on a Gel-Doc system (Bio-Rad, Italy). Band intensities were quantified by densitometry. TUBB/beta-tubulin (Santa Cruz Biotechnology, sc-9104; 1:1000) was used as a loading control.

Statistical analysis

Data are presented as mean ± SEM, geometric mean (25°-75° percentile), or fold change over control. Non-normally distributed variables were log transformed prior to analyses. Data were analyzed using the *t test* or ANOVA as appropriate. Least significant difference test was used for *post hoc* comparisons. P values <0.05 were considered statistically significant.

Disclosure statement

No potential conflict of interest was reported by the authors.

Funding

Barutta F. was the recipient of a Juvenile Diabetes Research Foundation Postdoctoral Fellowship (3-PDF-2014-109-A-N). The work was supported by the European Foundation for the Study of Diabetes (EFSD), the Ferrero Foundation (Alba), the University of Turin (ex. 60% grant) and the Italian Ministry for Education, University and Research (Ministero dell'Istruzione, dell'Università e della Ricerca - MIUR) under the program "Dipartimenti di Eccellenza 2018–2022" project D15D18000410001.

ORCID

F. Barutta http://orcid.org/0000-0001-9319-5123
S. Bellini http://orcid.org/0000-0002-2513-1651
E. Hirsh http://orcid.org/0000-0002-9073-6024
M. Martini http://orcid.org/0000-0002-4262-946X
G. Gruden http://orcid.org/0000-0001-8906-9589

References

[1] Alicic RZ, Rooney MT, Tuttle KR. Diabetic kidney disease: challenges, progress, and possibilities. Clin J Am Soc Nephrol. 2017 Dec 7;12(12):2032–2045. PubMed PMID: 28522654.
[2] Thomas MC, Brownlee M, Susztak K, et al. Diabetic kidney disease. Nat Rev Dis Primers. 2015 Jul 30;1:15018. PubMed PMID: 27188921.
[3] Dalla Vestra M, Masiero A, Roiter AM, et al. Is podocyte injury relevant in diabetic nephropathy? studies in patients with type 2 diabetes. Diabetes. 2003 Apr;52(4):1031–1035. PubMed PMID: 12663476.
[4] White KE, Bilous RW. diabiopsies study group.structural alterations to the podocyte are related to proteinuria in type 2 diabetic patients. PubMed PMID: 14993494. Nephrol Dial Transplant. 2004 Jun;19(6):1437–1440.
[5] Reidy K, Kang HM, Hostetter T, et al. Molecular mechanisms of diabetic kidney disease. J Clin Invest. 2014 Jun;124(6):2333–2340. PubMed PMID: 24892707.
[6] Kopp JB, Anders H-J, Susztak K, et al. Podocytopathies. Nat Rev Dis Primers. 2020 Aug 13;6(1):68. PubMed PMID: 32792490.
[7] Forbes JM, Cooper ME. Mechanisms of diabetic complications. Physiol Rev. 2013 Jan;93:137–188. PubMed PMID: 23303908.
[8] Brennan E, Kantharidis P, Cooper ME, et al. Pro-resolving lipid mediators: regulators of inflammation, metabolism and kidney function. Nat Rev Nephrol. 2021 Nov;17(11):725–739. PubMed PMID: 34282342.
[9] Gruden G, Cavallo Perin P, Camussi G. Insight on the pathogenesis of diabetic nephropathy from the study of podocyte and mesangial cell biology. Curr Diabetes Rev. 2005 Feb;1:27–40. PubMed PMID: 18220580.
[10] Zheng HJ, Zhang X, Guo J, et al. Lysosomal dysfunction-induced autophagic stress in diabetic kidney disease. J Cell Mol Med. 2020 Aug;24(15):8276–8290. PubMed PMID: 32583573.
[11] Tang C, Livingston MJ, Liu Z, et al. Autophagy in kidney homeostasis and disease. Nat Rev Nephrol. 2020 Sep;16(9):489–508. PubMed PMID: 32704047.
[12] Saxena S, Mathur A, Kakkar P. Critical role of mitochondrial dysfunction and impaired mitophagy in diabetic nephropathy. J Cell Physiol. 2019 Nov;234(11):19223–19236. PubMed PMID: 31032918.
[13] Lin Q, Banu K, Ni Z, et al. Podocyte autophagy in homeostasis and disease. J Clin Med. 2021 Mar 12;10(6):1184. PubMed PMID: 33809036.
[14] Forbes JM, Thorburn DR. Mitochondrial dysfunction in diabetic kidney disease. Nat Rev Nephrol. 2018 May;14(5):291–312. PubMed PMID: 29456246
[15] Audzeyenka I, Bierżyńska A, Lay AC. Podocyte bioenergetics in the development of diabetic nephropathy: the role of mitochondria. Endocrinology. 2022 Jan 1;163(1):bqab234. PubMed PMID: 34791124.
[16] Rustom A, Saffrich R, Markovic I, et al. Nanotubular highways for intercellular organelle transport. Science. 2004 Feb 13;303 (5660):1007–1010. PubMed PMID: 14963329.
[17] Dagar S, Pathak D, Oza HV, et al. Tunneling nanotubes and related structures: molecular mechanisms of formation and function. Biochem J. 2021 Nov 26;478(22):3977–3998. PubMed PMID: 34813650.
[18] Tiwari V, Koganti R, Russell G, et al. Role of tunneling nanotubes in viral infection, neurodegenerative disease, and cancer. Front Immunol. PubMed PMID: 34194434. 2021 Jun 14;12:680891.
[19] Zurzolo C. Tunneling nanotubes: reshaping connectivity. Curr Opin Cell Biol. 2021 Aug;71:139–147. PubMed PMID: 33866130.
[20] Cordero Cervantes D, Zurzolo C. Peering into tunneling nanotubes-The path forward. EMBO J. 2021 Apr 15;40(8): e105789. PubMed PMID: 33646572.
[21] Dupont M, Souriant S, Lugo-Villarino G, et al. Tunneling nanotubes: intimate communication between myeloid cells. Front Immunol. 2018 Jan 25;9:43. PubMed PMID: 29422895.
[22] Astanina K, Koch M, Jüngst C, et al. Lipid droplets as a novel cargo of tunnelling nanotubes in endothelial cells. Sci Rep. 2015 Jun 22;5:11453. PubMed PMID: 26095213.
[23] He K, Shi X, Zhang X, et al. Long-distance intercellular connectivity between cardiomyocytes and cardiofibroblasts mediated by membrane nanotubes. Cardiovasc Res. 2011 Oct 1;92(1):39–47. PubMed PMID: 21719573.
[24] Lou E, Zhai E, Sarkari A, et al. Cellular and molecular networking within the ecosystem of cancer cell communication via tunneling nanotubes. Front Cell Dev Biol. 2018 Oct 2;6:95. PubMed PMID: 30333973.
[25] Sartori-Rupp A, Cordero Cervantes D, Pepe A, et al. Correlative cryo-electron microscopy reveals the structure of TNTs in neuronal cells. Nat Commun. 2019 Jan 21;10(1):342. PubMed PMID: 30664666.
[26] Wittig D, Wang X, Walter C, et al. Multilevel communication of human retinal pigment epithelial cells via tunneling nanotubes. PLoS One. 2012;7(3):e33195. PubMed PMID: 22457742.
[27] Parker I, Evans KT, Ellefsen K, et al. Lattice light sheet imaging of membrane nanotubes between human breast cancer cells in culture and in brain metastases. Sci Rep. 2017 Sep 8;7(1):11029. PubMed PMID: 28887508.
[28] Weil S, Osswald M, Solecki G, et al. Tumor microtubes convey resistance to surgical lesions and chemotherapy in gliomas. Neuro Oncol. 2017;19:1316–1326. PubMed PMID: 28419303.
[29] Alarcon-Martinez L, Villafranca-Baughman D, Quintero H, et al. Interpericyte tunnelling nanotubes regulate neurovascular coupling. Nature. 2020;Sep 585 91–95. PubMed PMID: 32788726.
[30] Gabriel SS, Belge H, Gassama A, et al. Bone marrow transplantation improves proximal tubule dysfunction in a mouse model of dent disease. Kidney Int. 2017 Apr;91(4):842–855. PubMed PMID: 28143656.
[31] Hackl MJ, Burford JL, Villanueva K, et al. Tracking the fate of glomerular epithelial cells using serial in vivo multiphoton imaging in new mouse models with fluorescent lineage tags. Nat Med. 2013 Dec;19(12):1661–1666. PubMed PMID: 24270544.
[32] Lou E, Fujisawa S, Morozov A, et al. Tunneling nanotubes provide a unique conduit for intercellular transfer of cellular contents in human malignant pleural mesothelioma. PLoS One. 2012;7: e33093. PubMed PMID: 22427958.
[33] Wang Y, Cui J, Sun X, et al. Tunneling-nanotube development in astrocytes depends on p53 activation. Cell Death Differ. 2011; Apr;18 732–742. PubMed PMID: 21113142.
[34] Ranzinger J, Rustom A, Abel M, et al. Nanotube action between human mesothelial cells reveals novel aspects of

inflammatory responses. PLoS One. 2011;6:e29537. PubMed PMID: 22216308.
[35] Desir S, Dickson EL, Vogel RI, et al. Tunneling nanotube formation is stimulated by hypoxia in ovarian cancer cells. Oncotarget. 2016 Jul 12;7(28):43150–43161. PubMed PMID: 27223082.
[36] Zhang Y, Yu Z, Jiang D, et al. iPSC-mscs with high intrinsic miro1 and sensitivity to TNF-α yield efficacious mitochondrial transfer to rescue anthracycline-induced cardiomyopathy. Stem Cell Reports. 2016 Oct 11;7(4):749–763. PubMed PMID: 27641650.
[37] Zhu D, Tan KS, Zhang X, et al. Hydrogen peroxide alters membrane and cytoskeleton properties and increases intercellular connections in astrocytes. J Cell Sci. 2005 Aug 15;118(Pt 16):3695–3703. PubMed PMID: 16046474.
[38] Marlein CR, Zaitseva L, Piddock RE, et al. NADPH oxidase-2 derived superoxide drives mitochondrial transfer from bone marrow stromal cells to leukemic blasts. Blood. 2017 Oct 5;130 (14):1649–1660. PubMed PMID: 28733324.
[39] Gerdes HH, Carvalho RN. Intercellular transfer mediated by tunneling nanotubes. PubMed PMID: 18456488. Curr Opin Cell Biol. 2008 Aug;20(4):470–475.
[40] Marzo L, Gousset K, Zurzolo C. Multifaceted roles of tunneling nanotubes in intercellular communication. Front Physiol. 2012 Apr 10;3:72. PubMed PMID: 22514537.
[41] Pinto G, Saenz-de-Santa-Maria I, Chastagner P, et al. Patient-derived glioblastoma stem cells transfer mitochondria through tunneling nanotubes in tumor organoids. Biochem J. 2021 Jan 15;478(1):21–39. PubMed PMID: 33245115.
[42] Burt R, Dey A, Aref S, et al. Activated stromal cells transfer mitochondria to rescue acute lymphoblastic leukemia cells from oxidative stress. Blood. 2019 Oct 24;134(17):1415–1429. PubMed PMID: 31501154.
[43] Abounit S, Bousset L, Loria F, et al. Tunneling nanotubes spread fibrillar α-synuclein by intercellular trafficking of lysosomes. EMBO J. 2016 Oct 4;35(19):2120–2138. PubMed PMID: 27550960.
[44] Sáenz-de-Santa-María I, Bernardo-Castiñeira C, Enciso E, et al. Control of long-distance cell-to-cell communication and autophagosome transfer in squamous cell carcinoma via tunneling nanotubes. Oncotarget. 2017 Mar 28;8(13):20939–20960. PubMed PMID: 28423494.
[45] Hase K, Kimura S, Takatsu H, et al. M-Sec promotes membrane nanotube formation by interacting with Ral and the exocyst complex. Nat Cell Biol. 2009 Dec;1112:1427–1432. PubMed PMID: 19935652.
[46] Kimura S, Yamashita M, Yamakami-Kimura M, et al. Distinct roles for the N- and C-terminal regions of m-sec in plasma membrane deformation during tunneling nanotube formation. Sci Rep. 2016 Sep 15;6:33548. PubMed PMID: 27629377
[47] Kimura S, Hase K, Ohno H. Tunneling nanotubes: emerging view of their molecular components and formation mechanisms. Exp Cell Res. 2012 Aug 15;318(14):1699–1706. PubMed PMID: 22652450.
[48] Hashimoto M, Bhuyan F, Hiyoshi M, et al. Potential role of the formation of tunneling nanotubes in HIV-1 spread in macrophages. J Immunol. 2016 Feb 15;196(4):1832–1841. PubMed PMID: 26773158.
[49] Jia L, Shi Y, Wen Y, et al. The roles of TNFAIP2 in cancers and infectious diseases. J Cell Mol Med. 2018 Nov;2211:5188–5195. PubMed PMID: 30145807.
[50] Wolf FW, Sarma V, Seldin M, et al. B94, a primary response gene inducible by tumor necrosis factor-a, is expressed in developing hematopoietic tissues and the sperm acrosome. J Biol Chem. 1994 Feb 4;269(5):3633–3640. PubMed PMID: 8106408.
[51] Rusiniak ME, Yu M, Ross DT, et al. Identification of B94 (TNFAIP2) as a potential retinoic acid target gene in acute promyelocytic leukemia. Cancer Res. 2000 Apr 1;60(7):1824–1829. PubMed PMID: 10766166.
[52] Sarma V, Wolfe FW, Marks R, et al. Cloning of a novel tumor necrosis factor-alpha-inducible primary response gene that is differentially expressed in development and capillary tube-like formation in vitro. J Immunol. 1992 May 15;148(10):3302–3312. PubMed PMID: 1374453.
[53] Li J, Song Y, Yu B, et al. TNFAIP2 promotes non-small cell lung cancer cells and targeted by miR-145-5p. DNA Cell Biol. 2020 Jul;397:1256–1263. PubMed PMID: 32456459.
[54] Barutta F, Kimura S, Hase K, et al. Protective role of the M-sec-tunneling nanotube system in podocytes. J Am Soc Nephrol. 2021 May 3;32(5):1114–1130. PubMed PMID: 33722931.
[55] Papeta N, Zheng Z, Schon EA, et al. Prkdc participates in mitochondrial genome maintenance and prevents adriamycin-induced nephropathy in mice. J Clin Invest. 2010 Nov;120(11):4055–4064. PubMed PMID: 20978358.
[56] Zheng Z, Schmidt-Ott KM, Chua S, et al. A mendelian locus on chromosome 16 determines susceptibility to doxorubicin nephropathy in the mouse. Proc Natl Acad Sci USA. 2005 Feb 15;102 (7):2502–2507. PubMed PMID: 15699352.
[57] Watanabe M, Takahashi Y, Hiura K, et al. A single amino acid substitution in PRKDC is a determinant of sensitivity to adriamycin-induced renal injury in mouse. Biochem Biophys Res Commun. 2021 Jun 4;556:121–126. PubMed PMID: 33839407.
[58] Barutta F, Bruno G, Grimaldi S, et al. Inflammation in diabetic nephropathy: moving toward clinical biomarkers and targets for treatment. Endocrine. 2015 Apr;48(3):730–742. PubMed PMID: 25273317.
[59] Bork T, Liang W, Yamahara K, et al. Podocytes maintain high basal levels of autophagy independent of mtor signaling. Autophagy. 2020 Nov;16(11):1932–1948. PubMed PMID: 31865844.
[60] Mizushima N, Yamamoto A, Matsui M, et al. In vivo analysis of autophagy in response to nutrient starvation using transgenic mice expressing a fluorescent autophagosome marker. Mol Biol Cell. 2004 Mar;15(3):1101–1111. PubMed PMID: 14699058.
[61] Liu WJ, Gan Y, Huang WF, et al. Lysosome restoration to activate podocyte autophagy: a new therapeutic strategy for diabetic kidney disease. Cell Death Dis. 2019 Oct 24;10(11):806. PubMed PMID: 31649253.
[62] Woo CY, Kc R, Kim M, et al. Autophagic flux defect in diabetic kidney disease results in megamitochondria formation in podocytes. Biochem Biophys Res Commun. 2020 Jan 15;521 (3):660–667. PubMed PMID: 31679688.
[63] Vallon V, Rose M, Gerasimova M, et al. Knockout of Na-glucose transporter SGLT2 attenuates hyperglycemia and glomerular hyperfiltration but not kidney growth or injury in diabetes mellitus. Am J Physiol Renal Physiol. 2013 Jan 15;304(2):F156–167. PubMed PMID: 23152292.
[64] Kitada M, Takeda A, Nagai T, et al. Dietary restriction ameliorates diabetic nephropathy through anti-inflammatory effects and regulation of the autophagy via restoration of sirt1 in diabetic wistar fatty (fa/fa) rats: a model of type 2 diabetes. Exp Diabetes Res. 2011;2011:908185.PubMed PMID: 21949662.
[65] Tagawa A, Yasuda M, Kume S, et al. Impaired podocyte autophagy exacerbates proteinuria in diabetic nephropathy. Diabetes. 2016 Mar;65(3):755–767. PubMed PMID: 26384385.
[66] Ji J, Zhao Y, Na C, et al. Connexin 43-autophagy loop in the podocyte injury of diabetic nephropathy. Int J Mol Med. 2019 Nov;44(5):1781–1788. PubMed PMID: 31545399.
[67] Mostafa DK, Khedr MM, Barakat MK, et al. Autophagy blockade mechanistically links proton pump inhibitors to worsened diabetic nephropathy and aborts the renoprotection of metformin/enalapril. Life Sci. 2021 Jan 15;265:118818. PubMed PMID: 33275985.
[68] Liu WJ, Shen TT, Chen RH, et al. Autophagy-lysosome pathway in renal tubular epithelial cells is disrupted by advanced glycation end products in diabetic nephropathy. J Biol Chem. 2015 Aug 14;290(33):20499–20510. PubMed PMID: 26100632.
[69] Yang D, Livingston MJ, Liu Z, et al. Autophagy in diabetic kidney disease: regulation, pathological role and therapeutic potential. Cell Mol Life Sci. 2018 Feb;75(4):669–688. PubMed PMID: 28871310.

[70] Liu J, Li QX, Wang XJ, et al. β-Arrestins promote podocyte injury by inhibition of autophagy in diabetic nephropathy. Cell Death Dis. 2016 Apr 7;7(4):e2183. PubMed PMID:27054338.
[71] Zhao X, Chen Y, Tan X, et al. Advanced glycation end-products suppress autophagic flux in podocytes by activating mammalian target of rapamycin and inhibiting nuclear translocation of transcription factor EB. J Pathol. 2018 Jun;245(2):235–248. PubMed PMID: 29570219.
[72] Lenoir O, Jasiek M, Hénique C, et al. Endothelial cell and podocyte autophagy synergistically protect from diabetes-induced glomerulosclerosis. Autophagy. 2015;11(7):1130–1145. PubMed PMID: 26039325.
[73] Li L, Liu Y, Li S, et al. Signal regulatory protein α protects podocytes through promoting autophagic activity. JCI Insight. 2019 Mar 19;5(9):e124747. PubMed PMID: 30888336.
[74] Gödel M, Hartleben B, Herbach N, et al. Role of mTOR in podocyte function and diabetic nephropathy in humans and mice. J Clin Invest. 2011 Jun;121(6):2197–2209. PubMed PMID: 21606591.
[75] Ma Z, Li L, Livingston MJ, et al. p53/microRNA-214/ULK1 axis impairs renal tubular autophagy in diabetic kidney disease. J Clin Invest. 2020 Sep;130(9):5011–5026. PubMed PMID: 32804155.
[76] Lee YH, Kim SH, Kang JM, et al. Empagliflozin attenuates diabetic tubulopathy by improving mitochondrial fragmentation and autophagy. Am J Physiol Renal Physiol. 2019 Oct;317(4):F767–F780. PubMed PMID: 31390268.
[77] Oshima Y, Kinouchi K, Ichihara A, et al. Prorenin receptor is essential for normal podocyte structure and function. J Am Soc Nephrol. 2011 Dec;22(12):2203–2212. PubMed PMID: 22052048.
[78] Yamamoto-Nonaka K, Koike M, Asanuma K, et al. Cathepsin D in podocytes is important in the pathogenesis of proteinuria and CKD. J Am Soc Nephrol. 2016 Sep;27(9):2685–2700. PubMed PMID: 26823550.
[79] Sun X, Wang Y, Zhang J, et al. Tunneling-nanotube direction determination in neurons and astrocytes. Cell Death Dis. 2012 Dec 6;3(12):e438. PubMed PMID: 23222508.
[80] Ranzinger J, Rustom A, Heide D, et al. The receptor for advanced glycation end-products (RAGE) plays a key role in the formation of nanotubes (NTs) between peritoneal mesothelial cells and in murine kidneys. Cell Tissue Res. 2014 Sep;357(3):667–679. PubMed PMID: 24870978.
[81] Tosi G, Vilella A, Chhabra R, et al. Insight on the fate of CNS-targeted nanoparticles. Part II: intercellular neuronal cell-to-cell transport. J Control Release. 2014Mar;177:96–107. PubMed PMID: 24417968.
[82] Rustom A. The missing link: does tunnelling nanotube-based supercellularity provide a new understanding of chronic and lifestyle diseases? Open Biol. 2016 Jun;6(6):160057. PubMed PMID: 27278648.
[83] Dilsizoglu Senol A, Samarani M, Syan S, et al. α-Synuclein fibrils subvert lysosome structure and function for the propagation of protein misfolding between cells through tunneling nanotubes. PLoS Biol. 2021 Jul 20;19(7):e3001287. PubMed PMID: 34283825.
[84] Zhang K, Sun Z, Chen X, et al. Intercellular transport of Tau protein and β-amyloid mediated by tunneling nanotubes. Am J Transl Res. 2021 Nov 15;13(11):12509–12522. PubMed PMID: 34956469.
[85] Osteikoetxea-Molnár A, Szabó-Meleg E, Tóth EA, et al. The growth determinants and transport properties of tunneling nanotube networks between B lymphocytes. Cell Mol Life Sci. 2016 Dec;73(23):4531–4545. PubMed PMID: 27125884.
[86] Onfelt B, Nedvetzki S, Benninger RK, et al. Structurally distinct membrane nanotubes between human macrophages support long-distance vesicular traffic or surfing of bacteria. J Immunol. 2006 Dec 15;177(12):8476–8483. PubMed PMID: 17142745.
[87] Naphade S, Sharma J, Gaide Chevronnay HP, et al. Brief reports: lysosomal cross-correction by hematopoietic stem cell-derived macrophages via tunneling nanotubes. Stem Cells. 2015 Jan;33(1):301–309. PubMed PMID: 25186209.
[88] Victoria GS, Zurzolo C. The spread of prion-like proteins by lysosomes and tunneling nanotubes: implications for neurodegenerative diseases. J Cell Biol. 2017 Sep 4;216(9):2633–2644. PubMed PMID: 28724527.
[89] de Rooij B, Polak R, Stalpers F, et al. Tunneling nanotubes facilitate autophagosome transfer in the leukemic niche. Leukemia. 2017 Jul;31(7):1651–1654. PubMed PMID: 28400620.
[90] Unger T, Borghi C, Charchar F, et al. International society of hypertension global hypertension practice guidelines. J Hypertens. 2020 Jun;38(6):982–1004. PubMed PMID: 32371787.
[91] Dunn SR, Qi Z, Bottinger EP, et al. Utility of endogenous creatinine clearance as a measure of renal function in mice. Kidney Int. 2004 May;65(5):1959–1967. PubMed PMID: 15086941.